Star Peptide Polymers are Multi-Drug Resistant Gram-positive Bacteria Killers

Wenyi Li[1], Sara Hadjigol[1], Alicia Rasines Mazo[2], James Holden[3], Jason Lenzo[3], Steven J Shirbin[2], Anders Barlow[4], Sadegh Shabani[2], Tao Huang[5], Eric C. Reynolds[3], Greg G. Qiao[2*], Neil M. O'Brien-Simpson[1*]

[1]ACTV Research group, Melbourne Dental School, Centre for Oral Health Research, Royal Dental Hospital and The Bio21 Institute of Molecular Science and Biotechnology, The University of Melbourne, Victoria, 3010. Australia. [2]Polymer Science Group, Department of Chemical & Biomolecular Engineering, The University of Melbourne, Parkville, Victoria 3010, Australia, [3]Melbourne Dental School, Centre for Oral Health Research, Royal Dental Hospital and The Bio21 Institute of Molecular Science and Biotechnology, The University of Melbourne, Victoria, 3010. Australia. [4]Materials Characterisation and Fabrication Platform, Melbourne School of Engineering, University of Melbourne, Parkville, VIC 3010, Australia, and [5]Department of Biomedical Engineering, Melbourne School of Engineering, University of Melbourne, Parkville, VIC 3010, Australia.

*Neil O'Brien-Simpson and Greg Qiao

Email: neil.obs@unimelb.edu.au and gregghq@unimelb.edu.au

Abstract

Antibiotic resistance in bacteria, especially Gram-positive bacteria like *Staphylococcus aureus*, is gaining considerable momentum worldwide and unless checked will pose a global health crisis. With few new antibiotics coming on the market, there is a need for novel antimicrobial materials that target and kill multi-drug resistant (MDR) Gram-positive pathogens like Methicillin-resistant *Staphylococcus aureus* (MRSA). In this study, using a novel mixed-bacteria antimicrobial assay we show that the star-peptide polymers preferentially target and kill Gram-positive pathogens including MRSA. A major effect on the activity of the star-peptide polymer was structure, with an 8-armed structure inducing the greatest bactericidal activity. The different star-peptide polymer structures were found to induce different mechanisms of bacterial death both *in vitro* and *in vivo*. These results highlight the potential utility of peptide/polymers to fabricate materials for therapeutic development against MDR Gram-positive bacterial infections.

Keywords: Antibiotic, nanoengineered peptide polymer, Gram-positive, Staphylococcus aureus, antimicrobial resistance, membrane active

Introduction

Since their discovery, antibiotics have been hailed as wonder drugs, saving millions of lives and increasing society's quality of life [1]. However, the wide overuse of antibiotics in humans and animals has led to the emergence of multi-drug resistant (MDR) bacterial infections [2]. Compounding this issue is the small number of new antibiotics coming onto the market, as indicated in a 2014 report by the Pew Charitable Trust showing only 10 of 67 phase III clinical trials meeting the FDA criteria for approval for clinical application [3]. Most of these newly approved antibiotics were slight chemical variations on existing antibiotics, and bacterial resistance to these new antibiotics has been rapid, with resistance developing within a few years or less of their release onto the market [4-6]. Without novel antibiotics on the horizon through a nearly dry development pipeline, the management of MDR infections will become increasingly difficult. Without effective antimicrobial therapies it is predicted that mortality from bacterial infections will overtake cancer by 2050 [7]. Among the bacteria identified by the WHO as being major threats to human health, *Staphylococcus aureus*, and its respective multi-drug resistant strains such as methicillin resistant *S. aureus* (MRSA), are considered high priority pathogens for targeted drug development [8]. *S. aureus,* a Gram-positive pathogen, is one of the most common causes of hospital and community-acquired infections in humans, as it is widely present on the human body, including the skin, nose, gut, and bloodstream [9]. More importantly, the virulence factors and toxins released by this pathogen, as well as its wide distribution provide a high chance for infection and toxin-mediated disease, such as *staphylococcal* foodborne diseases and bacteraemia [10]. Since the introduction of β-lactam antibiotics, the emergence of MRSA across the world has had a negative impact on the clinical management of *S. aureus* infections which now place a large economic burden on society [11]. Although MRSA can still be treated in many infections by the use of powerful antibiotics – vancomycin,

daptomycin, linezolid and ceftaroline – there are now accounts of MRSA strains resistant to these last line of defence treatments [12-13].

To combat the increasing MDR crisis associated with *S. aureus*- and MRSA-related infections, novel anti-MRSA molecules are currently under pre-clinical and clinical investigation [14]. These novel antimicrobials inhibit peptidoglycan/cell membrane, protein synthesis, DNA synthesis and fatty acid synthesis. Amongst the antimicrobial materials being investigated to treat *S. aureus*/MRSA infections, amphiphilic and cationic polymers have emerged as a promising alternative to antibiotics as they broadly target bacterial cell envelopes or membranes with decreased potential for resistance onset [15-16]. Additionally, polypeptide-based antimicrobial agents have shown broad-spectrum activity and distinct modes of action [16-18]. Our group has previously developed a new class of star-shaped peptide polymers, termed "structurally nanoengineered antimicrobial peptide polymers" or "SNAPPs" using *N*-carboxyanhydride (NCA) ring opening polymerisation (ROP) of lysine and valine NCA monomers. SNAPPs were found to have superior antibacterial activity against Gram-negative pathogens compared to other materials (natural antimicrobial peptides), and were highly effective against MDR species both *in vitro* and *in vivo* [19-20]. Recently, several other groups have also shown that amphiphilic star-shaped polypeptides generated *via* NCA polymerisation are a promising new family of antimicrobial agents [21-30], as summarised in our recent reviews [15-16]. In comparison with linear, hinged and cyclic antibacterial polymers, the star architecture offers a highly cationic micro-environment [31], which may enhance the polypeptide's antibacterial activity *via* stronger electrostatic interaction with the target bacterial membranes. It is worth noting that most reported star-shaped amphiphilic peptide polymers exhibited potent activity against Gram-negative nosocomial and MDR bacteria. Our previous structure-activity studies against Gram-negative *Escherichia coli* revealed the arm density and arm length in the star-shaped SNAPPs have direct effects on the polymer's antimicrobial activity, with SNAPPs

of increasing arm number and length exhibiting enhanced activity[32]. To date the SNAPPs' efficacy has only been demonstrated against several critical priority Gram-negative pathogens, for instance *Acinetobacter baumannii*, *Escherichia coli* and *Pseudomonas aeruginosa* [21-24]. It is known that peptide structure and number of arms dramatically effects activity[33-34]. Thus, we hypothesize that different SNAPPs structures with different arm length and number can modulate their spectrum against bacteria. The key question is if such a star polypeptide can also be used to clear multi-drug resistant Gram-positive pathogens, such as *S. aureus*, a major pathogen challenge we are facing today.

Although previously we have shown that SNAPPs can kill Gram-negative bacteria[19, 32], here, we show that by modulating the SNAPPs structure and their number of arms and length, the rational designed SNAPPs can preferentially target and kill Gram-positive *S. aureus* and MRSA than Gram-negative *E. coli* in a polymicrobial assays. The therapeutic potential of structurally diverse SNAPPs was tested against Gram-positive MDR bacteria, *S. aureus* ATCC 29213 and MRSA ATCC 33591 both *in vitro* and *in vivo*. Our comprehensive study shows that SNAPPs are highly potent Gram-positive bactericidal materials and that specific structural elements favour activity. We also show that SNAPPs kill MRSA within minutes, induce stress responses and cause cytoplasmic membrane disruption, membrane potential loss and unregulated ion efflux/influx accompanied by dysregulation of efflux pumps.

Experimental details

SNAPPs synthesis

SNAPPs with varying core size (denoted as SX) and increasing degree of arm length (small/$_S$, medium/$_M$, long/$_L$, very-long/$_{VL}$) were synthesized via the grafting-from ring opening polymerization of NCAs as previously reported [32]. Briefly, the synthesis of S16$_L$ is described as an example. PAMAM-G2 with surface amino groups (10 mg, 3.07×10^{-3} mmol, 40 μL) was

firstly dried under vacuum to remove traces of methanol. Subsequently, the G2 initiator was redissolved in anhydrous DMSO (672 µL). To this solution placed under and Argon atmosphere, was added a solution of Nε-(benzyloxycarbonyl)-L-lysine NCA (300.8 mg, 0.982 mmol, 20 eq.) and D,L-valine NCA (70.3 mg, 0.49 mmol, 10 eq.) in anhydrous DMF, such that $[NCA]_0$ = 55 mg/mL. The reaction was allowed to proceed under exclusion of moisture by positive Ar flow, with temperature control afforded by the use of an insulated ice bath. Conversion was monitored by ^{1}H NMR and GPC analysis. Upon stagnation in conversion, the reaction mixture was quenched by addition of n-butanol in excess, followed by concentration in vacuo and precipitation of the polymer into ether. Deprotection of the SNAPPs was achieved through acid hydrolysis by treatment with HBr and trifluoroacetic acid (TFA) for 2 h as previously reported [32]. The deprotected peptide polymer was dialyzed against distilled water and lyophilized prior to ^{1}H NMR and GPC analyses for determination of amino acid composition and average molecular weight, respectively, prior to proceeding to biological testing. Detailed characterization of each SNAPP is provided in the supplementary information.

Bacterial growth conditions

The bacterial culture of *S. aureus* ATCC 29213, *S. aureus* ATCC33591 (MRSA) and *S. aureus* ATCC43300 (MRSA), *E. faecalis* ATCC 29212, MDR-*E. faecalis* ATCC 51575, *E. coli* BAA-8739, MDR-*E. coli* BAA-3051, *K. pneumoniae* ATCC 13883, MDR FADDI-KP028 were inoculated in 100% Mueller Hinton broth (MHB). Briefly, 1-2 colonies of a corresponding bacterium strain from an agar plate was suspended in 10 mL MHB and incubated overnight at 37°C. Then, 1 mL of the overnight culture was then re-inoculated into 20 mL of fresh MHB and incubated to the late exponential phase at 37°C. The late exponential phase culture was then used for the antibacterial assays, mode of action and in vivo studies.

Mixed culture CFU assay.

Single colonies of *S. aureus* and *E. coli* were inoculated into MHB broth and incubated overnight at 37°C. The following morning, 2% and 4% v/v inoculations of *E. coli* and *S. aureus*, respectively, were added to 10 mL of MHB and the cultures were grown for ~2.5-3 hours to late exponential phase. Following incubation, 1:100 dilutions of culture were stained with Syto9 and PI (1:1000) and counted on a Beckman Coulter Cytoflex flow cytometer. To perform the assay, cultures of *S. aureus* and *E. coli* were adjusted to 2×10^6 CFU/mL. Two-fold serial dilutions of SNAPPs were performed, starting at 100 µg/mL. Bacteria were added to a 96 well plate, 100µL of *E. coli* or *S. aureus* alone for the single culture experiments, 50µL of each *E. coli* and *S. aureus* for the mixed culture experiments (total of 100 µL). Dilutions of SNAPP (100 µL) were added to the bacterial cultures in the 96 well plate and the assay was incubated at 37°C for 90 minutes. Following the incubation, 10 × serial dilutions of each well was performed and 10 µL aliquots of the dilutions were spotted onto LB agar with or without Vancomycin (10 µg/mL) or Polymyxin B (12.5 µg/mL). Plates were incubated at 37°C for 24 hours and the viable bacteria enumerated.

Mixed culture flow cytometry assay.

Single colonies of *S. aureus*, *MRSA* and *E. coli* were inoculated into LB broth and incubated 37°C, 18 hr. Following incubation, 5% v/v, 5% v/v and 10% v/v inoculations of *E. coli*, *S. aureus* and *MRSA* respectively, were added to LB broth and the cultures were grown for ~1.5-2.5 hours to approximately so as to reach late exponential phase of growth. For the assay, 4×10^7 of each bacteria were taken from the late exponential cultures and centrifuged (7000 g, 10 min) and resuspended in 200 µL PBS (pH 8.3). *E. coli* and Gram-positive bacteria (*S. aureus* and *MRSA*) were incubated (37 °C, 30 min) with 20µL Atto647-NHS ester (Sigma-Aldrich, Cat# 07376-1MG-F) and 20µL AF488-NHS ester (Lumiprobe, Cat#21820), respectively. After incubation, bacteria were transferred to 50 mL Falcon tubes and top up to 20ml MHB broth

and centrifuged (7000 g, 10 min). The fluorescently labelled *S. aureus*, *MRSA* and *E. coli* were then adjusted to 2×10^6 CFU/mL by resuspending each bacteria with 10 ml MHB broth. A two-fold serial dilution of SNAPPs were performed, starting at 50 μg/mL, volume 100μL. Bacteria were added to the wells in the following formats, 50 μL of *S. aureus*, *MRSA* or *E. coli* alone for the single culture controls, 50 μL of each *S. aureus*, *MRSA* and *E. coli* for the mixed culture experiments (total of 100 μL), these being: *S. aureus* + *E. coli* and *MRSA* + *E. coli* all with and without SNAPP. The bacterial cultures/SNAPP mixtures were incubated at 37 °C for 30 minutes. Following the incubation, 100 μL of each well was stained with Propidium Iodide (PI) - 1.0 mg/mL Solution in Water (Invitrogen, Cat# P3566, 1:1000) and the level of membrane disruption as indicated by PI+ bacteria analysed on a Beckman Coulter Cytoflex flow cytometer.

Image of mixed culture

Single colonies of *S. aureus* and *E. coli* were inoculated into MHB broth and incubated overnight at 37 ºC. The following morning 2% and 4% inoculations of *E. coli* and *S. aureus*, respectively, were added to 10 mL of MHB and the cultures were grown for ~2.5-3 hours to approximately late exponential phase. Following incubation, 1:100 dilutions of culture were stained with Syto9 and PI (1:1000) and counted on a Beckman Coulter Cytoflex flow cytometer. 1×10^6 CFU of each 10 bacteria was stained with FM 4-64FX dye (Thermo Fisher) as per manufacturer's instructions. 1×10^6 of each labelled bacterium were mixed together and treated with 10 mg/mL of Atto488-labelled SNAPP and incubated for 90 minutes before being washed with DMEM. The bacteria suspension was then placed in a polylysine coated chambered coverglass slide (Thermo Fisher) and incubated for 60 minutes to allow the bacteria to settle and bind. Unbound bacteria were rinsed away with DMEM and the remaining bacteria fixed with 4% paraformaldehyde for 5 minutes at room temperature. The fixative was washed away with DMEM and the bacteria stored in SlowFade Diamond Antifade Mountant (Thermo

Fisher). Images were taken on the Deltavision OMX Structured Illumination Microscope V4 Blaze (Applied Precision). Images were produced using the ImageJ processing package (National Institutes of Health, USA).

Antibacterial assays

Each SNAPP was tested for antibacterial activity against the Gram-positive bacteria *S. aureus* and MRSA in 100% MHB. The minimum inhibitory concentration (MIC) and minimum bactericidal concentration (MBC) were determined, and microbial flow cytometry was used to monitor membrane integrity/permeability to the fluorescent dye PI (minimum membrane disruption concentration [MDC]) for each SNAPPs as previous described [35-36]. The MIC was determined by plotting maximal growth versus peptide concentration, according to the Lambert and Pearson analysis method [37-38], while MBC was confirmed via colony-forming unit (CFU) measuring assay. As for PG or LTA inhibition assay, a series of 50 μL dilutions of PG or LTA from 250 μg/mL to 4 μg/mL were added to a 96-well plate with prefilled 1×MIC of each SNAPPs (50 μL). After 30 min incubation, 100 μL of 2×10^6 cells/mL were added to the plate and incubation at 37°C, 90 min, followed by general MIC and MDC determination.

***In vivo* peritoneal infection model.**

All experiments involving animals were performed according to protocols approved by the University of Melbourne, Australia. Forty-five 6-8-week-old female C57/BL6 mice (9 groups; 5 animals per group, weighing ca. 25 g) were obtained from the Walter and Eliza Hall Institute of Medical Research Animal Services Unit, Melbourne, Australia. *S. aureus* or MRSA were grown as for the in vitro assays and mice were given an i.p. injection of 10^7 CFU of bacteria in PBS using a 25G needle. Mice were then treated with SNAPPs for 3 doses in MEM at 30min, 2 hours and 6 hours post bacterial inoculation, injecting 2.8 mg/kg mice of SNAPPs in PBS i.p. using a 25G needle. Mice were killed 24 hours post the bacterial inoculum, and the

peritoneal cavity washed with 3 mL of PBS and the peritoneal contents were aspirated. An aliquot of the lavage fluid was taken and serial dilutions were performed and plated onto LB agar to determine the residual bacterial load in the peritoneal cavity. The remainder of the peritoneal lavage was used to determine the neutrophil influx. Briefly, cells were harvested by centrifugation at 400 × g for 10 minutes before being resuspended in FACS buffer (PBS containing 1% (v/v) BSA and 0.05% (v/v) sodium azide). Cells were then incubated with Fc block (1:200; Becton Dickinson) for 20 minutes on ice before being stained with Ly6G-PE (1:200; Clone 1A8 (RUO), Cat# 551461, Becton Dickinson). Cells were then washed with FACS buffer before being analysed on the Cytoflex Flow Cytometer (Beckman Coulter). Neutrophils were identified as Ly6G positive cells.

Membrane potential assay

Membrane potential was determined by flow cytometry (CytoFLEX Flow Cytometer, Beckman Coulter) with a BacLight Bacterial Membrane Potential Kit (Invitrogen) as previous described [19, 35]. *S. aureus* and MRSA harvested at late exponential phase of growth were diluted to 2×10^6 cells/mL in MHB and 100 µL of this culture was added and mixed with serial dilution of SNAPPs (100 µL, 0.125×MBC, 0.25×MBC, 0.5×MBC, 1×MBC, 2×MBC) in a 96-well plate. The protonophore carbonyl cyanide-*m*-chlorophenylhydrazone (CCCP, final concentration 5 µM) was added to the non-treated bacteria to provide a depolarized population control. After 60 min incubation at 37°C, the 30 µM 3,3'-diethyloxa-carbocyanine iodide ($DiOC_2$) was added to all the tested samples, which associates in the inner membrane of bacteria and emits a green fluorescence in polarised (low membrane potential) bacterial cells. As the membrane potential becomes larger (moving towards a depolarised membrane) the DiOC2(3) dye aggregates causing a red shift in fluorescence. Membrane potential was determined by flow cytometer as a ratio of the fluorescent cells between the red and green fluorescence. Gates were drawn based on the controls present in normal cell population or depolarized regions (Figure S3 and S4).

Time-kill kinetic assay.

Time-kill kinetics of the SNAPPs were performed against *S. aureus* and MRSA and adapted from the ASTM time-kill kinetic assay [39]. The bacterial cells were harvested at late-logarithmic phase of growth and then re-suspended into MHB corresponding to 2×10^6 CFU/mL and then incubated with 2×MBC, 1×MBC, 0.5×MBC, 0.25×MBC, 0.1×MBC SNAPPs at 37°C. 10 μL of aliquot were removed from the treated bacterial suspensions at specific time intervals (0, 1, 5, 10, 15, 20, 40, 60, and 120 min) and plated on the LB-agar plates to determine CFU/mL. Following incubation for 12–14 h at 37°C, colonies were then counted. Two independent experiments were performed to calculate the mean value of CFU formation.

Fluorometric efflux activity determination

The designed direct efflux activity assay was determined by utilising flow cytometry (CytoFLEX Flow Cytometer, Beckman Coulter). *S. aureus* and MRSA were harvested and washed at the late exponential phase to prepared 2×10^6 cells/mL in PBS only. 100 μL of bacteria culture in PBS was added to pre-filled 96-well plate with serial dilution of SNAPPs (50 μL in PBS) for 30 min incubation at 25°C, as well as three control groups filled with PBS. Then, a 50 μL EtBr solution (4 μg/mL in PBS) was added to the mixture for an additional 30 min incubation at 25°C. After the second incubation, the bacterial cells were pelleted by centrifugation (4500 g, 10 min) and the pellet was resuspended into 100 μL PBS to remove extracellular SNAPPs/EtBr remaining in the culture. Then the SNAPPs treated wells added with additional 50 μL PBS and 50 μL glucose solution, which can reenergise the efflux pump and lead accumulated EtBr to efflux out of the cells, while three control groups were added with 50 μL CCCP (10 μg/mL) + 50 μL PBS or 50 μL CCCP + 50 μL glucose (10%) or 50 μL glucose + 50 μL PBS. After mixing, the plate was subjected to flow cytometry analysis. As intracellular EtBr-DNA binding resulted in fluorescence (excitation and emission filters of

528/2 and 590/2 nm respectively), gates were drawn based on controls and fluorescent wavelength.

Isothermal calorimetric titration analysis (ICT)

Microcalorimetric measurements of SNAPPs binding to LPS, LTA or PG were performed on a Malvern MicroCal PEAQ isothermal titration calorimeter (ITC). The *E. coli* LPS with SNAPPs,; *S. aureus* LTA or *S. aureus* PG with SNAPPs were separately dissolved in 20 mM HEPES (pH 7.0). The control experiments, background interaction, were performed by titrating LPS. LTA or PG (32.5 μM) into 20 mM HEPES with 13 × 3 μL injections at 150 s intervals from a 42 μL injection syringe, where the contents were stirred constantly at 750 rpm at 37 °C. The ITC binding experiments were determined by titrating LPS, LTA or PG (32.5 μM) into SNAPPs (1.63 μM in 20 mM HEPES) with 13 × 3 μL injections. The total heat signal from each injection was determined as the area under the individual peaks and plotted versus the [cell membrane components]/[SNAPPs] molar ratio. The normalised data were analyzed to determine number of binding sites (n), and molar change in enthalpy of binding (ΔH) by nonlinear least-squares regression analysis in terms of an equation series that define two sets of independent sites.

ROS production determination

ROS production induced by SNAPPs treatment was analysed by using CellROX deep red reagent with flow cytometry using protocols previously described[19]. Briefly, the cells were harvested and viable cells were diluted into 2 × 10^6 cells/mL in MEM. A 100 μL aliquot of bacteria culture in MEM was added to pre-filled 96-well plate with serial dilution of SNAPPs (100 μL in PBS, 0.25×MBC, 0.5×MBC, 1×MBC, 2×MBC) for a 90 min incubation at 37°C. The bacterial culture was then stained with CellROX deep red reagent (C10422, Thermo Fisher Scientific Australia) and Syto9 reagent (S34854, Thermo Fisher Scientific Australia) and

subjected to CytoFLEX Flow Cytometer (Beckman Coulter). The CellROX® Deep Red reagent will become fluorescent after the oxidation by intracellular ROS (Figure S5). Gates were drawn based on the controls present in untreated cell population without significant ROS generation of the Syto9 labelled bacteria (Green channel 525-40 nm), while the CellROX deep red reagent labelled bacterial population (Red channel 660-10 nm) represent ROS generation.

Helium Ion Microscopy

The morphologies of bacterial strain methicillin-sensitive S. aureus ATCC 29213 and MRSA after treatment with S8m and S16m was observed using Helium Ion Microscopy (HIM, Zeiss, Germany). The samples were prepared in the following steps. Firstly, 100 μL of 4×MBC, 2×MBC, 1×MBC, 0.5×MBC S8m and S16m in PBS solution were added to each well of 96-well microplates, 100 μL pure PBS was used as untreated control. Afterwards, 100 μL MHB with 1×10^7 cell/mL bacteria was added to each well. After 90 min incubation, 10 μL of both treated and untreated bacteria were pipetted on clean glass cover slides, then put them into oven with temperature of 37 °C for 20-30 min to dry. The dried samples were transferred to 12-well plate, 2.5% glutaraldehyde (v/v) was added to each well to fix the bacteria cells for 1 h and wash with PBS gently, then gradient ethanol solution (30%, 50%, 60%, 70%, 80%, 90%, 95% and 100%) was used for dehydration for 10 mins each time. The prepared samples were dried in the fume hood, overnight, before use. The coverslips were then mounted onto standard pin stubs using double-sided adhesive carbon tape and inserted into the HIM in preparation for imaging. No further sample preparation was required. Imaging was performed using a 25 keV He^+ ion beam with a typical beam current of 0.8-1.0 pA. Charge neutralisation was achieved *in situ* via a low energy electron flood gun optimised for each sample.

Results

SNAPPs preparation and antimicrobial activity.

A SNAPP library was synthesized via NCA ROP, employing polyamidoamine (PAMAM) dendrimer cores of different generations (G0, G1, G2), to furnish star polypeptides with 4, 8, and 16 arms, respectively using our previously described methods [32]. The dendritic macroinitiators with free primary amine functionality allowed the facile ring opening polymerization of lysine and valine NCAs at reduced temperatures; furthermore, by altering the monomer to initiator ratio we were able to fabricate SNAPPs of different arm lengths. Thus, we obtained SNAPPs SX_S, SX_M, SX_L, SX_{VL} where X denotes the number of arms and the subscripts provide an indication of the length of the arm (small, 5-12 amino acids (aa), medium, 12-18aa, large, 18-25aa, very large, 25-31aa). Examples of the characterization of $S16_M$ are provided in Figure S1 and S2. The resultant SNAPP polypeptide library was readily water soluble upon hydrolytic cleavage of the protecting group in the lysine side chain, furnishing peptide polymers ranging in molecular weight from 3 kDa to 53 kDa and their physiochemical properties characterised (Table S1). The SNAPPs could be stably stored in aqueous solutions for testing against Gram-positive and Gram-negative bacteria in the *in vitro* antimicrobial assays.

We initially compared the antimicrobial activity of our previously identified potent Gram-negative bactericidal SNAPP, S16 ($S16_M$). against WHO critical and high threat Gram-negative and Gram-positive bacteria (**Table 1**). Antibacterial activity was measured in undiluted/unmodified Mueller-Hinton broth (MHB) with activity presented as minimum inhibitory concentration (MIC) or minimum bactericidal concentration (MBC) [35-36], providing SNAPP efficacy on inhibiting bacterial growth (MIC) and bactericidal activity (MBC). Although the SNAPPs can form aggregates in MHB medium, we have previously shown this only partially effects that antimicrobial activity[19], $S16_M$ and $S8_M$ were found to have sub-

micromolar activity against the Gram-positive antibiotic susceptible and multi-drug resistant (MDR) strains of *S. aureus* and *Enterococcus faecalis* (**Table 1**). This activity was equivalent or stronger than that found for the Gram-negative MDR strains of *Escherichia coli* and *Klebsiella pneumoniae*. We then tested the SNAPP analogue $S8_M$ and found it too was highly active against the antibiotic sensitive and MDR strains of *S. aureus* and *E. faecalis* when compared with the Gram-negative strains tested.

Table 1*. The antibacterial activity of SNAPPs against Gram-positive and Gram-negative bacteria.*

Bacteria	SNAPP $S8_M$		SNAPP $S16_M$	
	MIC_{90} (μg/mL (μM))	MBC (μg/mL (μM))	MIC_{90} (μg/mL (μM))	MBC (μg/mL (μM))
S. aureus	22.1±0.3 (0.94)	31.5±0.9 (1.35)	39.7±3.1 (0.97)	35.4±0.7 (0.86)
MRSA	12.0±0.2 (0.51)	24.7±4.1 (1.06)	22.4±0.7 (0.55)	36.2±4.2 (0.88)
E. faecalis	23.5±0.35 (1.00)	15.9±0.18 (0.68)	20.4±0.42 (0.50)	16.5±0.01 (0.40)
MDR-*E. faecalis*	20.6±0.34 (0.88)	16.0±0.05 (0.68)	23.6±0.17 (0.57)	16.7±0.21 (0.41)
E. coli	13.5±1.13 (0.58)	14.0±0.08 (0.60)	12.8±0.01 (0.31)	8.2±0.04 (0.34)
MDR-*E. coli*	25.8±0.99 (1.10)	15.5±0.14 (0.66)	26.0±0.09 (0.63)	15.3±0.33 (0.37)
K. pneumoniae	32.7±12.59 (1.40)	31.5±2.55 (1.35)	48.0±2.47 (1.17)	28.2±0.11 (0.69)
MDR-*K. pneumoniae*	98.2±12.77 (4.20)	63.2±0.67 (2.70)	51.4±0.96 (1.25)	54.3±0.01 (1.32)

Following on from these findings that SNAPPs had potent Gram-positive activity on parity with activity towards Gram-negative bacteria we hypothesised that in a mixed culture assay SNAPPs may preferentially target one bacteria over the other. Generally, it is rare for bacteria to be found *in vivo* as a single species and are typically found in/on the human body as polymicrobial communities [40]. Such polymicrobial infections are managed by non-specific treatment with antibacterial agents, which can damage beneficial commensal microbes. Therefore, it is important to study the effect of the presence of bystander bacteria, which may bind SNAPPs to varying degrees, and the effect they may have on the effectiveness to target the desired bacteria. We initially conducted confocal microscopy to show preferential binding of SNAPP $S16_M$ to either a representative Gram-positive bacterium, *S. aureus*, or Gram-negative bacteria, *E. coli*, (labelled with FM 4-64FX, a lipophilic styryl dye that fluoresces

intensely upon binding to the cytoplasmic membrane (red)). The bacteria were mixed in equal numbers and treated with Atto488-labelled $S16_M$ (green). *E. coli* and *S. aureus* were differentiated from each by morphology, rod versus cocci respectively, and binding of SNAPP was identified as a yellow overlay. SNAPP $S16_M$ was found to preferentially bind to the Gram-positive *S. aureus* in a mixed culture with Gram-negative *E. coli* (**Figure 1**). *S. aureus* is seen as the predominately yellow cocci compared to the red (no SNAPP) rods of *E. coli*.

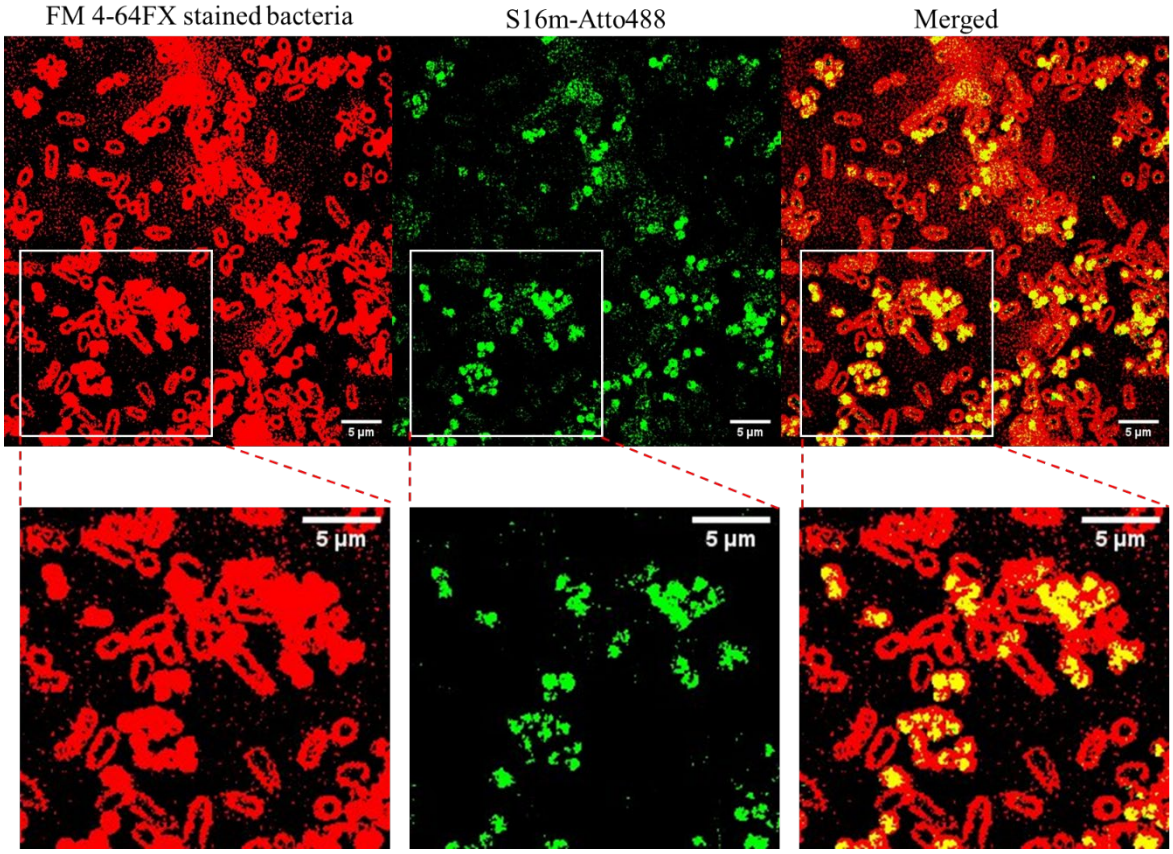

Figure 1. *Labelled $S16_M$ treated mixed culture of S. aureus (cocci shape) and E. coli (rod shape). The $S16_M$ was labelled with Atto488 (green), while the bacteria culture was stained with the fixable FM 4-64FX dye (red).*

Bactericidal activity of $S8_M$ and $S16_M$ in mixed cultures.

Here, we designed a mixed-culture assay of representative Gram-negative bacteria, *E. coli* or *K. pneumoniae* with the Gram-positive species, *S. aureus*. Following harvesting at late

exponential phase of growth, a co-inoculum of equal numbers of *E. coli (*or *K. pneumoniae)* and *S. aureus* was incubated with a serial dilution of either $S8_M$ or $S16_M$ and the CFU for each bacteria determined by using selective media to determine preferential killing. **Figure 2** shows that when *E. coli (*or *K. pneumoniae)* and *S. aureus* were mixed and treated with either $S8_M$ or $S16_M$, there was no change in the ability of either SNAPP in their ability to kill *S. aureus* in polymicrobial culture compared to the *S. aureus* monoculture. However, in a polymicrobial culture there was a reduced ability of $S8_M$ and $S16_M$, in killing *K. pneumoniae* whereas there was an increased ability to kill *E. coli* (Figure 2). This differential in Gram-negative bacterial killing (*K. pneumoniae* and *E. coli*) and not Gram-positive (*S. aureus*) in a polymicrobial culture indicates that SNAPPs preferentially target Gram-positive bacteria as activity to Gram-negative bacteria can fluctuate depending on the presence of other bacteria. At the low concentration of SNAPPs, the preferential killing of *S. aureus* over *E. coli* was 12-20 fold. This species preference may be due to the surface charge (zeta potential) of the bacteria as *S. aureus* has a more negative zeta potential of -37.1mV compared with *E. coli* of -12.7mV [41]. As SNAPPs have a strong positive charge due to the lysine residues in the polymer arms they would be more attracted to the great negatively charged *S. aureus* than *E. coli*. This finding provides insight into the structure/function relationship of the SNAPPs which may be used to modify their design to improve efficacy in future studies.

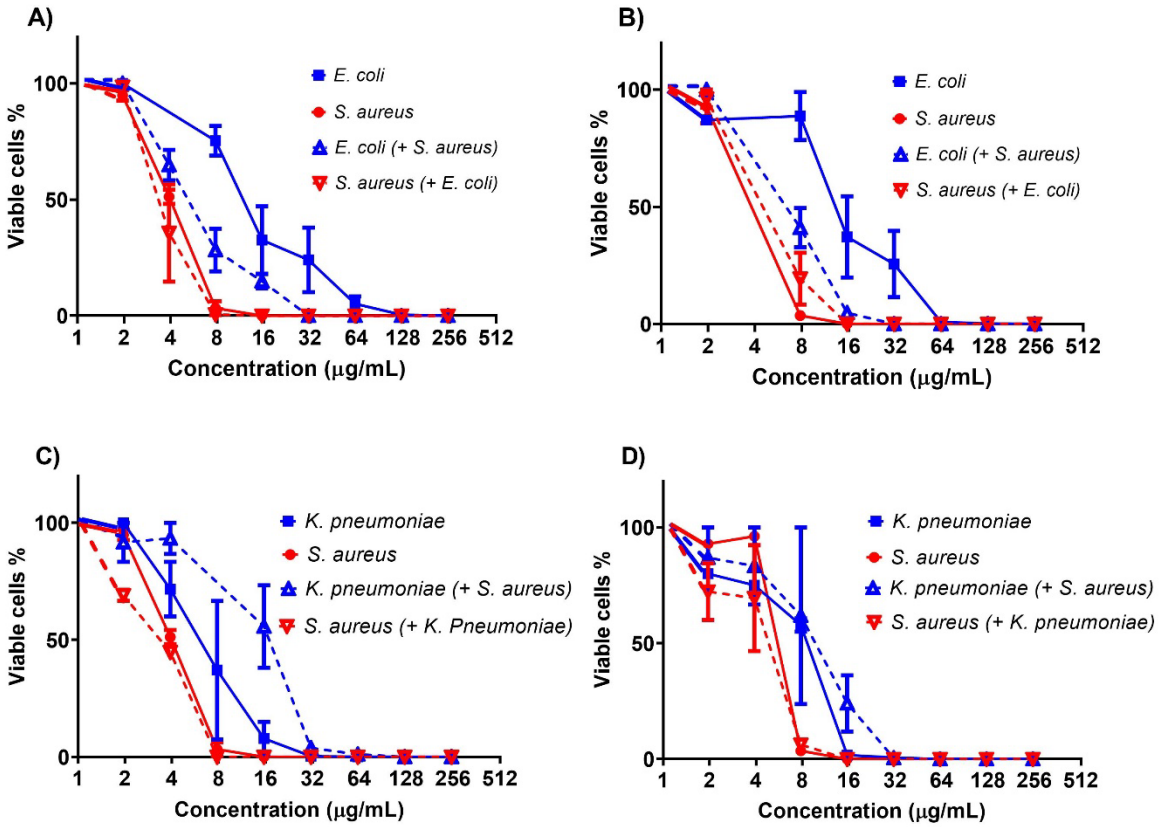

Figure 2. *SNAPPs preferentially killed S. aureus in a polymicrobial MBC assay. MBC assays were performed on a 1:1 mixture of E. coli and S. aureus (A & B), or K. pneumoniae and S. aureus (C & D), while the LB agar plate containing Polymyxin B for the CFU of S. aureus (+E. coli or + K. pneumoniae) and LB agar plate with Vancomycin showed the CFU of E. coli or K. pneumoniae (+S. aureus). The solid blue and red lines represent E. coli (or K. pneumoniae) monoculture and S. aureus monoculture. A). The difference of CFU counts under* $S8_M$ *treatments of mixed culture of E. coli and S. aureus. B). The difference of CFU counts under* $S16_M$ *treatment of mixed culture of E. coli and S. aureus. C). The difference of CFU counts under* $S8_M$ *treatments of mixed culture of K. pneumoniae and S. aureus. D). The difference of CFU counts under* $S16_M$ *treatment of mixed culture of K. pneumoniae and S. aureus.*

To further investigate the finding of the preference of $S8_M$ and $S16_M$ to target *S. aureus* in the presence of *E. coli* (**Figure 2**), we developed a flow cytometry-based assay to monitor simultaneously the ability of either $S8_M$ or $S16_M$ to disrupt the cell membranes of bacteria in a

mixed inoculum of *S. aureus/E. coli* and *MRSA/E. coli* (**Figure 3**). Following harvesting at late exponential phase of growth, equal numbers of Atto647-labelled *E. coli* with either Alexafluor488-labelled *S. aureus* or MRSA were incubated with a serial dilution of either $S8_M$ or $S16_M$, and the level of membrane disruption of each bacterium was determined using propidium iodide (PI) by microbial flow cytometry. **Figure 3** clearly shows that incubation/treatment of the mixed bacterial cultures with $S8_M$ and $S16_M$ induced greater cell lysis of *S. aureus* than *E. coli* within the 30 minutes of the assay incubation. Furthermore, the MDC values of the labelled *S. aureus* or MRSA were always lower in a mixed culture with *E. coli* (Table S2). In a mixed *S. aureus/E. coli* culture $S8_M$ induced 24% more killing of *S. aureus* and 27% less killing of *E. coli* when compared with the killing of single bacterial cultures. $S8_M$ also induced 10% more killing of MRSA and 42% less killing of *E. coli* in the mixed cultures when compared with the killing of single bacterial cultures. (Table S2). Although $S16_M$ also showed a preference towards *S. aureus* or MRSA over *E. coli* in a mixed culture, the preference was weaker than that displayed by $S8_M$, inducing only 4% more killing of *S. aureus* and 47% less killing of *E. coli*. Furthermore, $S16_M$ produced no significant increase in killing of MRSA and only 12% less killing of *E. coli* in the respective mixed culture (Table S2). It was noted that there was variation in the activity between $S16_M$ and $S8_M$, particularly for *S. aureus* and MRSA, indicating that SNAPP structure may play a role in the targeting and activity of the SNAPPs.

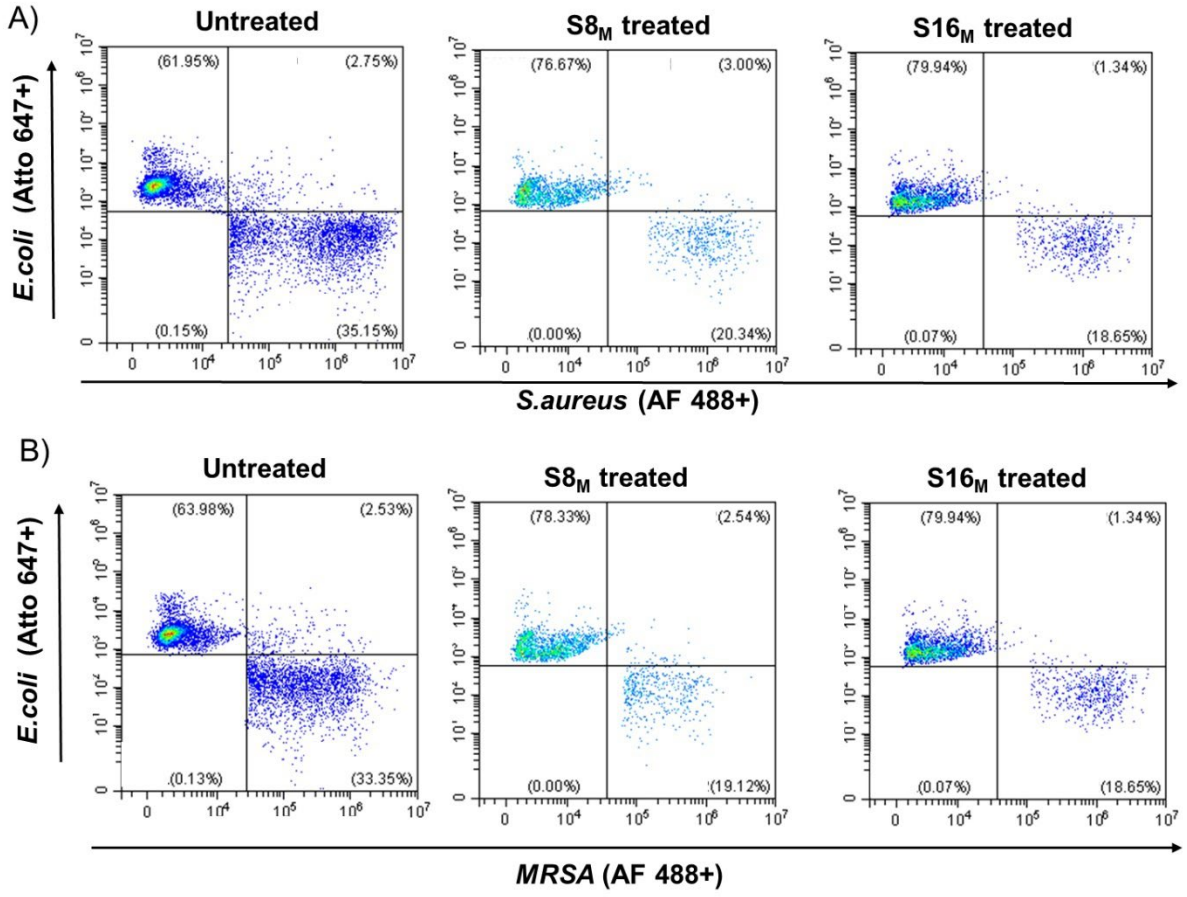

Figure 3. *Representative flow cytometry graphs of the proportion of bacteria following treatment with $S8_M$ or $S16_M$ in a mixed culture assay. Atto647 labelled E. coli were separating in vertical direction, while the S. aureus (A) or MRSA (B) were labelled with AF488 in horizontal direction. The PI positive population were gated with channel (525-40 nm for AF488 and 660-10 nm for Atto647) in comparison with SNAPP untreated samples.*

Effect of SNAPP structure on activity towards antibiotic-sensitive and MDR strains of *S. aureus*.

To investigate whether SNAPP structure affected antibacterial activity against *S. aureus* and MRSA the *in vitro* activity (MIC, MBC and membrane disruption concentration (MDC)) of the S4, S8 and S16 analogues was determined (**Table 2**). For the S4 analogues, the $S4_S$ had significantly ($p<0.01$) weaker activity against *S. aureus* and MRSA compared to $S4_M$, $S4_L$ and $S4_{VL}$, whilst $S4_M$ had significantly ($p<0.01$) weaker activity than $S4_L$ and $S4_{VL}$. The increase

in arm length for $S4_{VL}$ compared to $S4_L$ did not result in a significant improvement in antimicrobial activity. Taken together the longer arm S4 analogues $S4_L$ and $S4_{VL}$ had 5-8 fold greater activity than the short arm counterparts $S4_S$ and $S4_M$ against *S. aureus* and MRSA (**Table 2**). No significant difference in activity was found for the S8 or S16 analogues (**Table 2**), indicating that arm length and arm number in these higher order SNAPPs has little effect on activity against *S. aureus* or MRSA. In comparing the activity induced by SNAPP analogues of the same arm length but differing arm number, $S4_M$ and $S4_L$ had significantly ($p<0.01$) weaker activity compared to $S8_M$ or $S16_M$ and $S8_L$ or $S16_L$, respectively. The weaker activity observed with the S4 analogues compared to S8 and S16 analogues could be mitigated by an increase in arm length, as the activity of $S4_{VL}$ was comparable to the activity of the S8 and S16 SNAPP $_M$ and $_L$ analogues.

All the SNAPP analogues were found to induce membrane disruption of *S. aureus* and MRSA as indicated by the uptake of PI in the microbial flow cytometry assays (Table S3). The S8 and S16 analogues as well as the S4 analogues $S4_L$ and $S4_{VL}$ had the lowest and comparable (not significantly different) MDC values (**Table 2**). For S4 analogues, arm length had a significant effect on their ability to disrupt the cytoplasmic membrane with activity following the pattern $S4_s < S4_M < S4_L = S4_{VL}$. The MDC value of $S4_M$ was significantly ($p<0.05$) weaker than the S8 and S16 analogues with the same arm length ($S8_M$ and $S16_M$), indicating that an increase in arm number of the SNAPPs enhances membrane disruption. In addition, MIC was found to be equivalent to MBC, indicating the action of the SNAPPs is bactericidal (**Table 2**). With MDC being equivalent to MIC and MBC values, it suggests the mode of action for the SNAPPs leading to bacterial cell death was disruption and/or alteration of function of the cytoplasmic membrane of *S. aureus* and MRSA. Moreover, we further determined their activity against another MRSA strain ATCC43300, which also showed strong inhibition and bactericidal activity (**Table 2**).

***Table 2**. The antibacterial activity of SNAPPs against S. aureus and MRSA.*

SNAPPs	MW kDa	*S. aureus*			MRSA ATCC 33591			MRSA ATCC43300		
		MIC (μM)[a]	MBC (μM)[a]	MDC (μM)[a]	MIC (μM)[a]	MBC (μM)[a]	MDC (μM)[a]	MIC (μM)[a]	MBC (μM)[a]	MDC (μM)[a]
$S4_S$	3.3	32.3±1.0	39.0±0.9	15.9±2	28.0±2	37.3±2.8	25.8±3.5	—	—	—
$S4_M$	8.8	3.1±0.2	4.1±.06	1.5±0.2	2.7±0.1	3.0±0.2	1.8±0.5	—	—	—
$S4_L$	14.1	1.7±0.2	1.8±0.2	0.5±0.1	0.9±0.2	1.6±0.2	0.7±0.04	—	—	—
$S4_{VL}$	19.2	1.1±0.1	1.4±0.1	0.4±0.1	0.8±0.1	0.7±0.1	0.5±0.03	—	—	—
$S8_M$	23.4	1.0±0.01	1.0±0.03	0.4±0.08	0.6±0.01	0.9±0.2	0.5±0.01	1.5±0.1	2.3±0.02	2.8±0.1
$S8_L$	43.4	0.8±0.02	0.8±0.01	0.4±0.01	0.7±0.05	0.7±0.05	0.6±0.1	-	-	-
$S16_M$	41.1	1.0±0.1	0.8±0.01	0.4±0.01	0.6±0.01	0.8±0.1	0.4±0.03	1.0±0.04	1.4±0.04	1.5±0.04
$S16_L$	52.6	0.7±0.02	0.9±0.02	0.4±0.02	0.6±0.03	0.7±0.02	0.5±0.1	-	-	-
Methicillin	0.38	4.9±0.1	57.7±4.1	n.o.[b]	>328	>328	n.o.[b]	>328	>328	n.o.[b]
Gentamicin	0.48	—	—	—	—	—	—	≥70		n.o.[b]

a - the data were analysed in duplicate assays, n =2, and values in μg/mL are provided in Table S3; b - n.o. -membrane disruption was not observed.

Time-kill kinetics of $S8_M$ and $S16_M$

It is evident from the above data that the SNAPPs are potent antimicrobial agents. To further explore the antimicrobial efficiencies of the SNAPPs, we adapted the ASTM time-kill kinetic assay [39] to determine the SNAPP's bactericidal kinetics, where our adaption was the inclusion of a series of SNAPP concentrations (2×MBC, 1×MBC, 0.5×MBC, 0.25×MBC, 0.1×MBC) to be incubated with *S. aureus* and MRSA for specific time points. It should be noted that the minimum time to sample and plate for CFU analysis per test was 1 min. At the 2×MBC concentration $S8_M$ reduced *S. aureus* survival within 1 min by 2.68 log (>99%) and MRSA survival by 1.34 log (>95%) (**Figure 4**A, B). At 1×MBC a one-min incubation with $S8_M$ was found to reduce *S. aureus* survival by 2.16 log (>99%) and MRSA survival by 1.17 log (>93%) (**Figure 4**A, B). A 2×MBC concentration of $S16_M$ at one-min reduced survival of *S. aureus* and MRSA by a similar level to that of $S8_M$ (2×MBC), being 2.68 log (>99%) and 2.05 log (>99%) respectively (**Figure 4**C, D). However, within 1 min the activity of $S16_M$ at 1×MBC was significantly ($P<0.05$) weaker than that of $S8_M$ (1×MBC), reducing survival by 0.15 log (>29%) and 0.1 log (>20%) respectively (**Figure 4**C, D). Using a 3-log (99.9%) reduction in survival and zero CFU as a basis for bactericidal activity and sterility, respectively, a 1×MBC

concentration of $S8_M$ was both bactericidal and induced sterility for *S. aureus* at 10 mins. For MRSA the same occurred at 5 and 30 minutes, respectively. At the same concentration of 1×MBC, $S16_M$ took longer than $S8_M$ to be bactericidal and induced sterility for *S. aureus* at 10 and 90 mins, whereas for MRSA the same required 60 and 90 minutes. Taken together, $S8_M$ possesses a faster killing rate for both *S. aureus* and MRSA than $S16_M$ which is an important parameter to be considered for clinical applications and drug development.

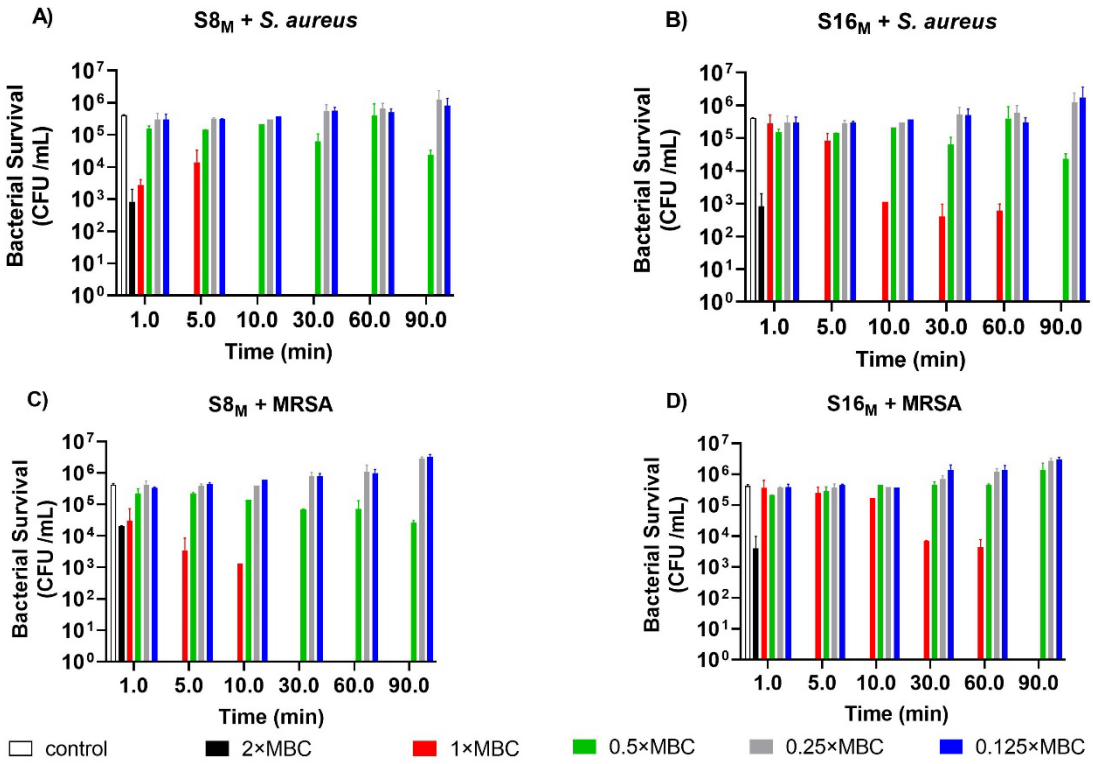

Figure 4. *Time kill-kinetics assay for SNAPPs against S. aureus and MRSA. Survival of S. aureus (A) and MRSA (C) incubated with $S8_M$ at differing times and concentrations. Survival of S. aureus (B) and MRSA (D) incubated with $S16_M$ at differing times and concentrations. Data representative of 2 biological replicates with 2 technical replicates/assay.*

Membrane potential studies

The cytoplasmic bacterial membrane plays a vital role in nutrient uptake, waste material excretion, micro-environment regulation, and is a major energy source for bacterial cells as the

ion motive force enables the transport of ions across the membrane [42]. Given that SNAPPs disrupt the membrane of *S. aureus* and MRSA, we hypothesised that SNAPPs would depolarise the cytoplasmic membrane and that this would correlate to the bactericidal concentration (MBC) of each SNAPP. To test this hypothesis, we analysed the ability of SNAPPs to alter the membrane potential of *S. aureus* and MRSA using a microbial flow cytometric method to evaluate membrane potential changes as we have previously described [19, 35]. *S. aureus* and MRSA were incubated with each SNAPP analogue at serial MBC concentrations (2×MBC, 1×MBC, 0.5×MBC, 0.25×MBC, 0.1×MBC 0.06×MBC), followed by staining with the membrane potential (ion sensitive/responsive) fluorophore 3,3'-diethyloxacarbocyanine iodide ($DiOC_2(3)$) and the membrane potential changes were compared to control bacteria that were, untreated and treated with the proton ionophore, carbonyl cyanide m-chlorophenyl hydrazone (CCCP) (**Figure 5**). The flow cytometry graphs show that all the SNAPPs had a strong effect on membrane potential of *S. aureus* and MRSA in comparison with the normal membrane potential state (without CCCP) and fully depolarized state (with CCCP) bacteria (Figure S3 and S4). **Figure 5** clearly shows that all of the S8 and S16 analogues induced complete membrane depolarisation of *S. aureus* and MRSA at 0.5×MBC concentration. At 0.25×MBC, the $S8_M$ and $S16_L$ also resulted in complete membrane depolarisation, but $S8_L$ and $S16_M$ only resulted in partial depolarisation, indicating that the arm length and arm number for the S8 and S16 play a role in their ability to depolarise bacterial membranes. At concentrations below 0.25×MBC, only the $S16_L$ induced membrane depolarisation that was significantly ($p<0.05$) higher than the untreated control. For the S4 analogues, arm length was found to be critical in effecting membrane potential with increasing arm length positively correlating to membrane depolarisation for both *S. aureus* and MRSA (**Figure 5**). Of the S4 analogues, only $S4_{VL}$ induced complete depolarisation of *S. aureus* and MRSA cytoplasmic membrane below the MBC value, at 0.5×MBC. The $S4_S$, $S4_M$, and $S4_L$ all induced partial membrane depolarisation

at 0.5×MBC, which increased at 1× and 2×MBC, with the pattern of activity being $S4_S$ < $S4_M$ < $S4_L$ << $S4_{VL}$. Complete membrane depolarisation was achieved at 1×MBC for the $S4_L$ and at 2×MBC for the $S4_M$. Taken together these data suggest that arm number in a SNAPP has a greater role than arm length in membrane potential depolarisation, although this may have an optimal point around an 8 arm SNAPP. It also shows that arm length can mitigate to some extent a reduction in arm number of a SNAPP, to effect complete depolarisation. Further, it indicates that by controlling arm number and length it is possible to optimise the SNAPPs to induce complete membrane depolarisation. It is known that the interaction of cationic antibiotics with the cytoplasmic membrane can cause K^+ leakage and lead to membrane potential changes [43]. While a similar effect may occur upon treatment with SNAPPs, membrane depolarisation is not the only mechanism leading to bacterial cell death as bacteria are known to alter their membrane potential temporarily to survive an external stimuli or stressors [42, 44].

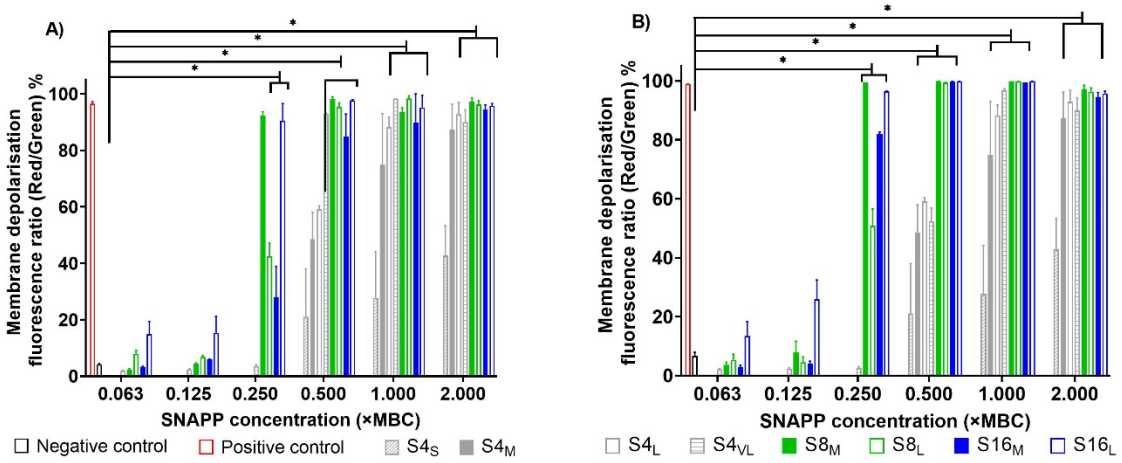

Figure 5. *Membrane potential of S. aureus (A) and MRSA (B) treated by SNAPPs. CCCP (a proton ionophore) was applied as the positive control to depolarise cells and untreated samples were used for negative control to show normal cell population. (* $p<0.05$), n=2.*

Reactive oxygen species generation

Bacteria alter their membrane potential due to environmental stressors such as exposure to antimicrobial materials, adjuvants and antibiotics. This alteration leads to the induction of a stress response in bacteria and the generation of reactive oxygen species (ROS). This response aids bacterial survival or achieve the induction of cell death *via* the oxidative damage-mediated pathway [42, 44-45]. The ability of antimicrobial materials to generate ROS that cause oxidative damage to cell wall components, DNA, RNA and cellular macromolecules, is a mechanism for enhancing bacterial cell death [46]. To investigate if the SNAPP analogues were able to induce ROS production, *S. aureus* and MRSA were incubated with SNAPPs, and ROS production was determined by microbial flow cytometry using CellROX® Deep Red as previously described [19, 35]. For both *S. aureus* and MRSA, the S4 analogues did not induce significant amounts of ROS (**Figure 6**), although $S4_{VL}$ did induce a significant ($p<0.05$) amount of ROS at 1×MBC for *S. aureus* (**Figure 6**A). In contrast, the $S8_M$, $S8_L$, $S16_M$ and $S16_L$ all induced a strong ROS response in *S. aureus* and MRSA at the sub-lethal concentration of 0.5×MBC and above (1× and 2×MBC). Further, the $S16_M$ and $S16_L$ were able to induce significant ($p<0.05$) ROS production at 0.25×MBC (**Figure 6**). There was a significant ($p<0.05$) decrease in the S8 and S16 analogues induction of ROS at 2×MBC which might be caused by rapid cell lysis and death during the incubation period at this concentration, resulting in the bacteria having a shorter period to form a stress response and produce ROS. The ability of SNAPPs to induce ROS at sub-lethal concentrations indicates that SNAPPs facilitate the induction of an oxidative damage-mediated death pathway and enhance ROS accumulation in bacteria, heightening their antimicrobial efficacy [47].

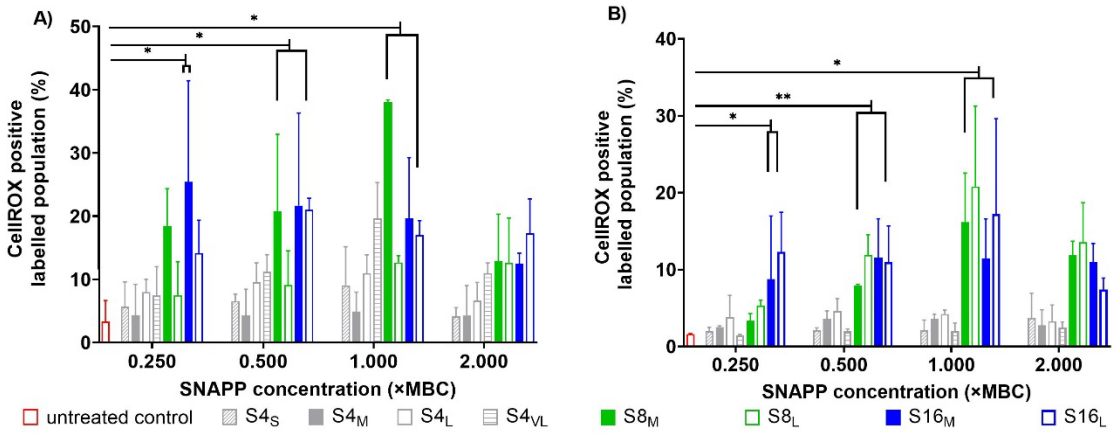

Figure 6. *SNAPPs induced ROS production of the percentage of S. aureus (A) and MRSA (B) cells stained with CellROX® red deep reagent. The representative graphs from flow cytometry of ROS analysis are provided in Figure S5. All data are expressed as mean ± standard deviation as indicated by the error bars (n = 4). *p<0.05, **p<0.01, Student's t test, significant difference from the untreated control.*

Effect of peptidoglycan and lipoteichoic acid on SNAPP antibacterial activity

From the MDC data (**Table 2**) it is apparent that the SNAPP analogues do efficiently interact with the cytoplasmic membrane of *S. aureus* and MRSA. As Gram-positive bacteria possess a thicker peptidoglycan (PG) layer than Gram-negative species then this thicker PG layer may contribute to the preferential attraction of the SNAPPs for the Gram-positive species. To affect the cytoplasmic membrane integrity the SNAPPs have to pass through the outer cell wall layer of the Gram-positive bacterium. We postulated that the SNAPPs may interact with peptidoglycan (PG) and/or lipoteichoic acid (LTA), the major components of the bacterial cell wall (Figure S6)[42] giving them a mechanism of attachment and entry into the bacterium, and this interaction may play a critical role in SNAPP efficacy against Gram-positive species.

To investigate whether SNAPPs interact with PG or LTA we co-incubated (30 mins) each SNAPP at their respective MIC with a serial dilution of PG or LTA (from *S. aureus* cell

envelope) prior to addition of *S. aureus* or MRSA. The inhibitory concentration (IC_{50}) was then determined (**Table 3** and Table S4) and the inhibition curves are shown in Figures S7, S8, S9 and S10. Both LTA and PG incubation with SNAPPs resulted in a decrease in the ability of SNAPPs to kill *S. aureus* and MRSA (**Table 3** and Table S4), with the biggest decrease in antibacterial activity seen when SNAPPs were incubated with LTA. The inhibitory action of LTA and PG was significantly ($p<0.05$) greater for MRSA than against *S. aureus*, as evidenced by the reduced antibacterial activity. Only a slight variation in the fold decrease in activity of SNAPPs incubated with PG was found, indicating that PG interaction is weak or may be generic for the SNAPPs. In contrast, LTA had a greater effect on inhibiting SNAPP antimicrobial activity towards *S. aureus* than PG, with a strong inhibitory activity observed with $S8_M$, $S8_L$ and $S16_M$. For anti-MRSA activity LTA inhibited $S8_M$ the most. As well as inhibiting activity, PG and to a greater extent LTA, inhibited the SNAPPs' ability to disrupt the cytoplasmic membrane (Table S4), indicating that the SNAPPs' ability to traverse the outer cell wall layer of *S. aureus* and MRSA was reduced.

It is known that PGs are polymeric carbohydrates interlinked by tetrapeptide residues to provide rigidity, while LTAs are amphipathic compounds with repeating lipidated glycerol phosphate, which intercalate into the cytoplasmic membrane (chemical structure illustrated in Figure S6) [48]. The loss of the membrane disruption caused by SNAPPs can be explained by the strong electrostatic interactions with the negatively charged moieties present on free LTA. This in turn would decrease the subsequent electrostatic interactions with bacteria, allowing them to maintain their membrane integrity. Together with the full loss of the SNAPPs' antibacterial activity in the presence of LTA (Figure S9 and Figure S10 A&C), the data suggested that SNAPPs bind to the amphipathic LTA, as a means of initial interaction before interacting with the cytoplasmic membrane. We hypothesise the strong interaction affinity of SNAPPs with LTA may allow the translocation of SNAPPs across the PG layer to the cytoplasmic membrane,

inducing pore formation, membrane lysis and cell death. The data above and the calculated therapeutic index (TI) of SNAPPs (Table S5), indicate that both $S8_M$ and $S16_M$ have the greatest impact on *S. aureus* and thus potential as lead clinical candidates and were chosen as the lead SNAPPs in the following studies.

Table 3. *Effect of lipoteichoic acid and peptidoglycan on SNAPP antibacterial activity against S. aureus and MRSA ATCC 33591.*

Lipoteichoic acid Inhibitory Concentration (IC50, µM)

SNAPP	*S. aureus*		MRSA ATCC 33591	
	IC50[a]	Fold decrease	IC50[a]	Fold decrease
$S4_S$	>37.90	>2.6	>37.90	>2.9
$S4_M$	4.4±0.10	3.1	>14.20	>11.5
$S4_L$	1.5±0.03	1.8	5.9±0.80	14.0
$S4_{VL}$	1.0±0.10	1.9	4.6±0.20	15.1
$S8_M$	2.4±0.10	5.0	4.1±0.01	16.1
$S8_L$	1.2±0.10	3.6	2.3±0.06	8.5
$S16_M$	1.4±0.02	3.0	>3.00	>11.1
$S16_L$	0.4±0.06	1.6	2.3±0.07	9.8

Peptidoglycan Inhibitory Concentration (IC50, µM)

SNAPP	*S. aureus*		MRSA ATCC 33591	
	IC50[a]	Fold decrease	IC50[a]	Fold decrease
$S4_S$	15.8±1.00	1.1	33.9±0.30	2.7
$S4_M$	2.6±0.05	1.9	2.6±0.04	2.2
$S4_L$	0.8±0.10	1.0	0.9±0.10	2.2
$S4_{VL}$	0.6±0.02	1.1	0.6±0.01	1.9
$S8_M$	0.9±0.20	1.8	0.5±0.02	2.1
$S8_L$	0.5±0.01	1.6	0.5±0.02	2.1
$S16_M$	0.6±0.02	1.2	0.6±0.01	2.2
$S16_L$	0.8±0.03	3.3	0.5±0.05	2.0

a = Data expressed as micro-molar concentrations calculated from three biological replicates containing two technical replicates per assay.

Determination of the binding interaction of SNAPPs with isolated bacterial cell wall components by ITC

In order to determine the binding affinity of SNAPPs with the membrane components from Gram-negative and Gram-positive bacteria, we performed isothermal titration calorimetry (ITC) to characterise their thermodynamic interaction by using direct titration of *E. coli* LPS; *S. aureus* LTA or *S. aureus* PG into SNAPPs. As Figure S11 shows, the titration curves indicated

an exothermic reaction upon the injection of LPS, LTA or PG into SNAPPs, except for the *S. aureus* PG into $S8_M$, where no binding activity was observed (Figure S11E). The determination of the K_D for each of the biomolecular interactions showed that both $S16_M$ and $S8_M$ had very low binding affinity constants (K_D), in the nanomolar range, towards *E. coli* LPS and *S. aureus* LTA, with around 1 binding site, indicating both SNAPPs had very strong binding to both LPS and LTA (This ability of $S8_M$ to bind to the surface of *S. aureus* and move quickly through the PG layer to the site of action as compared to $S16_M$ is reflected in the time kill and flow cytometry data that showed that $S8_M$ acts faster than $S16_M$ to kill *S. aureus*. Furthermore, circular dichroism analysis showed that $S8_M$ has a higher propensity to form an α-helical structure than $S16_M$ in a hydrophobic environment (20 % TFE) (**Figure S19** and **Table S6**) which would enhance its antimicrobial activity upon interacting with the highly hydrophobic inner membrane of Gram-positive bacteria. Despite the high binding to bacterial components and forming α-helical structures in hydrophobic environments, both SNAPPs had a very low effect on red blood cells (**Figure S20**) and with a haemolytic concentration >500μg/mL suggesting the SNAPPs have a high therapeutic index and a strong preference for bacteria rather than mammalian cells.

Table 4). For both LPS and LTA $S16_M$ had slightly strong binding (lower K_D) than $S8_M$, and significantly $S16_M$ had strong binding for PG, whereas $S8_M$ did not interact with PG and no binding was observed. These results suggest that $S16_M$ tends to have stronger affinity for the major cell wall components of both Gram-negative and Gram-positive bacteria than $S8_M$. These differences in binding affinities suggest different mechanisms of action for each SNAPP in killing bacteria. For $S16_M$ in killing *E. coli* (Gram-negative) as well as disrupting the inner membrane (primary site of action) it would have a greater disrupting effect on the LPS layer (outer layer/membrane)[19] than $S8_M$, which in turn would affect the bacteria as a whole leading to lower MICs and MBCs. Similarly, $S16_M$ has a stronger affinity for the components of the

outer layer (LTA and PG) of *S. aureus* which would retard it and so, slowing $S16_M$ course to the inner membrane. In contrast, $S8_M$ has the ability to target *S. aureus* after binding to LTA and with no affinity to PG, then moves, unimpeded, to the inner membrane where it disrupts it, leading to cell death. This ability of $S8_M$ to bind to the surface of *S. aureus* and move quickly through the PG layer to the site of action as compared to $S16_M$ is reflected in the time kill and flow cytometry data that showed that $S8_M$ acts faster than $S16_M$ to kill *S. aureus*. Furthermore, circular dichroism analysis showed that $S8_M$ has a higher propensity to form an α-helical structure than $S16_M$ in a hydrophobic environment (20 % TFE) (**Figure S19** and **Table S6**) which would enhance its antimicrobial activity upon interacting with the highly hydrophobic inner membrane of Gram-positive bacteria. Despite the high binding to bacterial components and forming α-helical structures in hydrophobic environments, both SNAPPs had a very low effect on red blood cells (**Figure S20**) and with a haemolytic concentration >500μg/mL suggesting the SNAPPs have a high therapeutic index and a strong preference for bacteria rather than mammalian cells.

Table 4. ITC assay data for the binding affinity of SNAPPs to E. coli LPS; S. aureus LTA or S. aureus PG. n as the number of binding sites and K_D is binding affinity constant.

	N (sites)	N (sites)	K_D (M)
$S8_M$	*E. coli* LPS	0.802	1.54E-08
$S16_M$		1.12	8.59E-09
$S8_M$	*S. aureus* PG	N/A	N/A
$S16_M$		0.726	7.43E-08
$S8_M$	*S. aureus* LTA	1.19	6.07E-08
$S16_M$		1.51	1.60E-08

SNAPP interactions with *S. aureus* and MRSA by Helium ion microscopy

Though multiple imaging methods are currently used to observe the interaction between antibacterial agents and cells via the use of fluorescence, we previously showed that attachment of fluorescent dyes to target compounds affects the physical properties and bioactivity of the compounds under investigation [19, 35]. The use of surface scanning microscopy, such as the

helium ion microscope (HIM) enables the direct study and analysis of biological samples with minimum sample damage at sub-nanometer resolution [49]. HIM also provides high spatial resolution, surface sensitivity, and the ability to image insulating surfaces such as biological specimens without the need for conductive coating that could otherwise mask the cell membrane damage. To directly observe the interactions between SNAPPs and bacterial cells, HIM was performed on an ORION NanoFab (Zeiss, Peabody MA) to study the morphologies of *S. aureus* and MRSA after their treatment with $S8_M$ and $S16_M$ at different concentrations (2×MBC, 1×MBC, 0.5×MBC, 0.25×MBC). The bacteria samples were loaded onto glass coverslips after 90 min incubation with SNAPPs, similar to our previous description[33, 50].

As can be seen in **Figure 7** there are distinct morphological changes in *S. aureus* and MRSA upon treatment with $S8_M$ and $S16_M$ at 1×MBC and 2×MBC concentrations, which resulted in membrane fragmentation, cytoplasmic content release and cellular disruption being observed in both bacteria. In contrast to untreated *S. aureus* and MRSA which have smooth spherical surfaces, SNAPP-treated bacteria displayed a rough and wrinkled cell surface, and membrane rupture at a sub-lethal dose of 0.5×MBC (**Figure 7**). Even at a much lower concentration (0.25×MBC), we observed cells that had clear signs of membrane distress. Interestingly, in several of the images, especially for MRSA, it is evident that there are small (80-100nm) spherical structures surrounding the damaged/rupturing bacteria, which are possibly membrane vesicles that have recently been reported to be produced by *S. aureus* [51]. This membrane vesicular response by MRSA and *S. aureus* to SNAPPs at low concentrations may be a method of defence against cytoplasmic membrane antimicrobials, as it could be hypothesized this would be an effective way to shed membrane lytic materials. These visual images of *S. aureus* and MRSA showing physical deformation and rupturing occurring at the same doses of SNAPP that have effects on the bacterial integrity/functioning (such as

generation of ROS, membrane disruption, efflux pump inhibition and cell death), demonstrate that SNAPPs dramatically affect bacterial cell integrity.

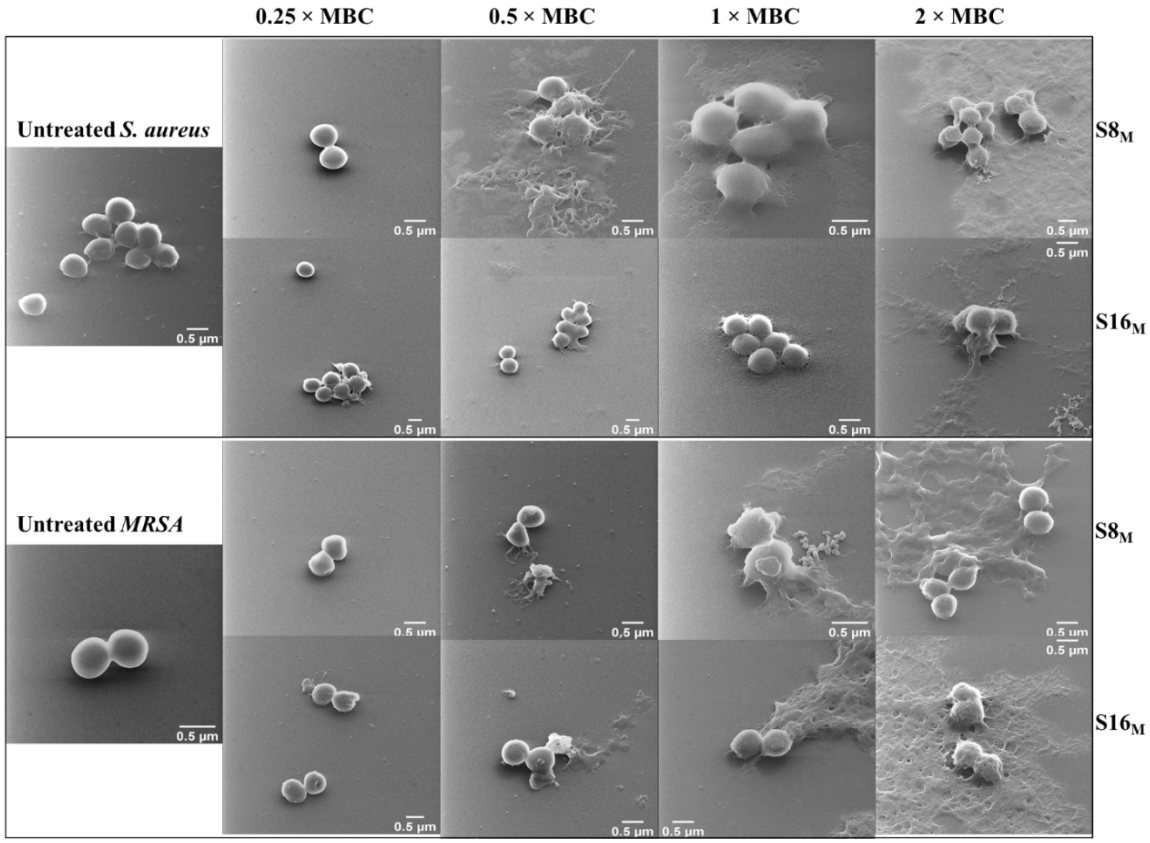

Figure 7. *HIM of the S. aureus and MRSA treated by $S8_M$ and $S16_M$ at different concentrations with untreated S. aureus or MRSA as controls.*

Efflux pump inhibition

Membrane potential is one of the main free energy sources powering efflux pumps through the transmembrane proton motive force (PMF) [52]. This is one of the mechanisms that is rapidly adapted in resistance to increase bacterial survival against antibiotics [53]. The high binding and depolarisation induced by $S8_M$ and $S16_M$ and their interaction with membrane components suggests they may also have an impact on efflux pump activity. Given the importance of porin/efflux pumps and the mechanism of some traditional antibiotics acting as ionophores, we further hypothesised that the $S8_M$ and $S16_M$ may abolish the PMF driving the

efflux pump by membrane depolarisation. To verify this, we designed a flow cytometric assay based on the ethidium bromide (EtBr, a fluorophore) accumulation method of assessing efflux pump activity [54-56], where the relative intracellular accumulation of EtBr reflects the efflux pump activity of a bacterium at a given time point. Higher levels of EtBr fluorescence within cells after a specific treatment are indicative of a decrease in efflux activity, and vice versa [57].

Bacteria at late exponential phase of growth were harvested, washed and then incubated in PBS containing no glucose to remove an energy source for efflux pumps. Bacteria were then incubated with the permanent proton ionophore (CCCP) or SNAPP or no treatment, then washed and resuspended in a glucose-containing buffer to re-energise the cells and efflux pump activity. The fluorescence intensity (EtBr+ bacteria) was then measured by flow cytometry to determine the effect of treatment on EtBr efflux. As can be seen in **Figure 8**, *S. aureus* or MRSA incubated with CCCP were unable to excrete EtBr upon addition of glucose compared to cells not treated with CCCP. *S. aureus* treated with $S8_M$ at 0.25 × MBC had higher EtBr concentrations and were unable to excrete EtBr when glucose was re-introduced into the media; a similar trend was observed for $S16_M$ starting at 0.5 × MBC (**Figure 8**A, 6B). By normalising the EtBr efflux fluorescence intensity with standard EtBr fluorescence background (CCCP-treated bacteria without glucose), we can clearly observe that the EtBr inside MRSA was unable to be excreted in presence of 0.5 × MBC $S8_M$ or $S16_M$, which is slightly higher than *S. aureus* with $S8_M$ (Figure S12). The inability of *S. aureus* or MRSA to excrete EtBr after $S8_M$ or $S16_M$ treatment indicated that SNAPPs bound firmly to the bacterial membrane to dissipate the PMF and inhibit the efflux activity.

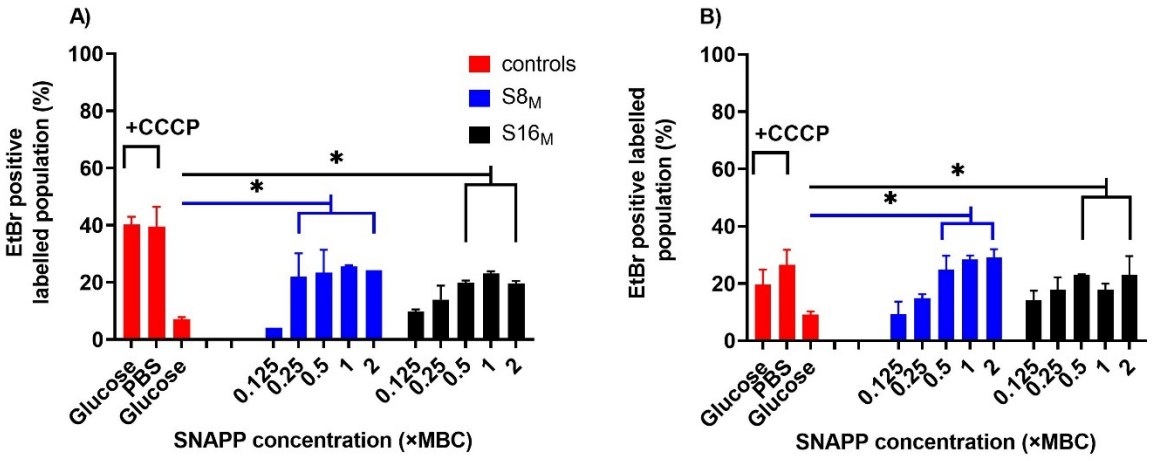

Figure 8. *EtBr efflux assay of S. aureus (A) and MRSA (B) under the treatment of $S8_M$ and $S16_M$ (*p<0.05), n=2. A), EtBr efflux assay in S. aureus; B), EtBr efflux assay in MRSA.*

Proposed mode of action against Gram-positive bacteria

Based on the detailed studies of the SNAPP antimicrobial activity towards Gram-positive bacteria, we propose a multistep model as to their mode of action, which involves binding to LTA and insertion of the SNAPPs into the cytoplasmic membrane. As illustrated in **Figure 9**, the interaction between SNAPPs and PG slightly contributes to their membrane interaction and can relate to their mode of actions, which is similar to some antimicrobial peptides and vancomycin[58]. Previously, we have shown the $S16_M$ can neutralise *E. coli* lipopolysaccharides (LPS) *in vitro*, a critical step for the SNAPP's action against Gram-negative bacteria[19]. Based on the structure similarity between LTA and LPS[59], the current results of high binding affinity with LTA (as indicated by external LTA inhibiting the antibacterial activity of SNAPPs) suggest the initial stage of SNAPP action toward Gram-positive species involves LTA binding thus targeting the SNAPPs to the bacterial surface. This is then followed by moving through the PG layer and then insertion into the cytoplasmic membrane to locally destabilise the membrane. As $S16_M$ strongly interacts with PG whereas $S8_M$ has no interaction, $S16_M$ would be retarded in the outer layer more than $S8_M$ and so have

a slower killing time. With imbedding into the inner membrane this interaction of the multi-peptide chains of SNAPPs may form a channel leading to ion efflux and bacterial membrane depolarisation, resulting in membrane fragmentation, rupture and cell lysis. Additionally, both $S8_M$ and $S16_M$ can act as ionophores to inhibit efflux pump activity to increase the intracellular concentration of SNAPPs. Furthermore, the ROS production under SNAPP treatment can likewise disrupt bacteria and lead to cell death.

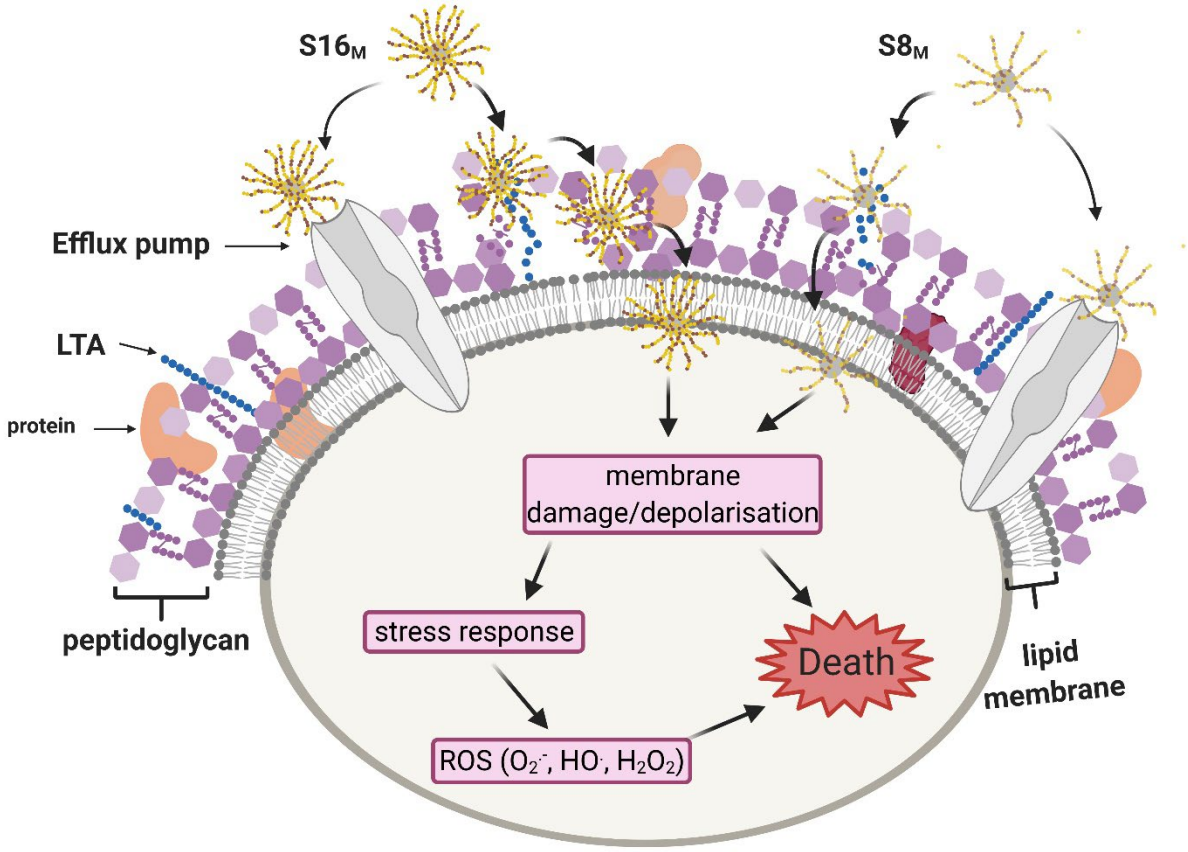

Figure 9. *Illustrated mechanism of the SNAPPs against Gram-positive bacteria.*

In vivo efficacy of $S8_M$ and $S16_M$ against *S. aureus* and MRSA infection

The major concern with antibiotic-resistant bacteria is their ability to cause systemic infections. Therefore, to further evaluate the efficacy of SNAPPs we have established an *in vivo* infection mouse model with *S. aureus* and MRSA. To evaluate the ability of $S8_M$ and $S16_M$ to control bacterial growth *in vivo*, mice were infected with a single peritoneal inoculation of

S. aureus or MRSA. Mice were then treated with 2.8 mg/kg of $S8_M$ or $S16_M$ at 0.5 h, 3 h and 6 h, or 50 mg/kg methicillin at the same time points. Mice that received either $S8_M$ or $S16_M$ had a significant reduction in peritoneal bacterial load, for both *S. aureus* and MRSA, when compared with the untreated infected control group (**Figure 10**A). For both $S8_M$ and $S16_M$-treated mice the reduction in CFU counts of 1.8 log (>98%) in both *S. aureus* and MRSA-infected mice was achieved, indicating that both SNAPPs have *in vivo* bactericidal activity. The protection afforded by treatment with either SNAPP ($S8_M$ and $S16_M$) was accompanied by a significant ($p<0.05$) neutrophil infiltrate into the peritoneal cavity of the treated animals which was not observed in the bacterial infection-alone or methicillin-treated groups (**Figure 10**B). Representative graphs of the flow cytometric analysis of neutrophils are provided in the supporting information (Figure S15-18). Treatment with methicillin resulted in sterility in the *S. aureus*-infected mice; however, for MRSA-infected mice there was an increase in CFU (0.25 log; 22%) when compared with the control infected group (**Figure 10**A). These results validate the model but also indicate that upon external pressure (such as methicillin) MRSA has enhanced growth *in vivo*.

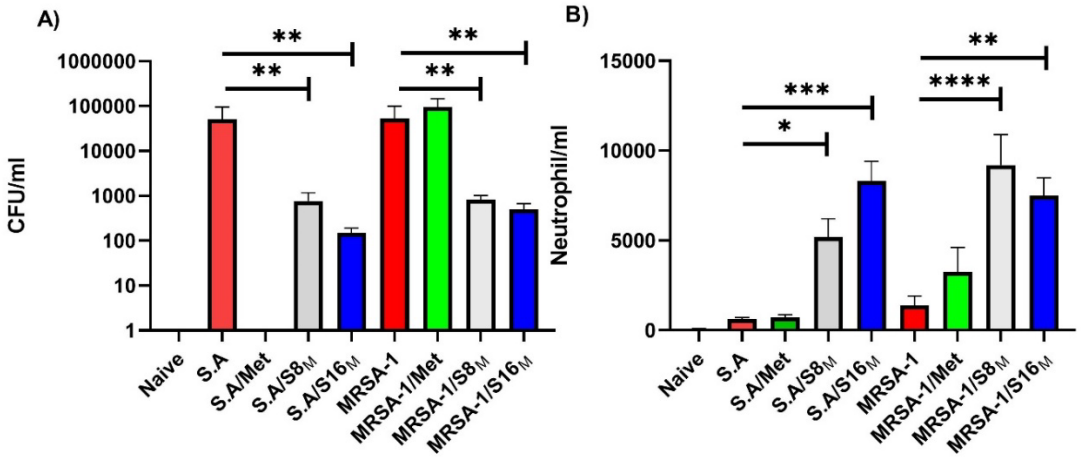

***Figure 10**. In vivo efficacy of SNAPPs S8M and S16M in a mouse peritonitis model. (A) CFU of S. aureus ATCC 29213 and MRSA ATCC 33591 found in the peritoneal wash of infected*

*mice 24 h after mock (MEM) treatment or treatment with methicillin (50 mg/Kg) or S8M or S16M (2.8 mg/kg). (B) Numbers of peritoneal neutrophils in the mild peritonitis model with mice 24 h after infection with S. aureus ATCC 29213 and MRSA ATCC 33591 found in the peritoneal wash of infected mice 24 h after mock (MEM) treatment or treatment with methicillin (50 mg/kg) or S8M or S16M (2.8 mg/kg). All data are expressed as mean ± s.d. (indicated by error bars), based on values obtained from five biological replicates (n=5). *p<0.05 **p<0.01, ***p< 0.001, Student's t-test, significant difference from the mock (MEM) control group test groups.*

The results of the peritoneal infection model indicate that both $S8_M$ and $S16_M$ control a peritoneal infection of both antibiotic-susceptible and resistant *S. aureus* strains. This reduction in bacterial load correlated with an increase in the neutrophil influx into the peritoneum. It is unclear if the observed reduction in bacterial load was a result of the direct killing of bacteria by both $S8_M$ and $S16_M$ or an increase in the bacterial killing by the recruited neutrophils, or a combination of both. Our previous work on SNAPPs demonstrated that direct killing and indirect activity via neutrophil recruitment was involved in combating Gram-negative infections *in vivo*, in these studies SNAPPs were shown to not induce inflammatory mediators, but did induce a localised increase in ATP which is a known neutrophil recruitment factor[32]. It has been shown that antimicrobial peptides are often more effective *in vivo* than *in vitro* and that this boosted activity has been accredited to the immunomodulatory properties of AMPs that affect neutrophil or macrophage differentiation, activation and phagocytic ability[5, 60]. A study conducted in our lab using MDR Gram-negative bacteria has shown that binding of inflammatory LPS by $S16_M$ inhibits macrophage NF-κB and inflammasome activation[19]. However, these anti-inflammatory effects may be specific for SNAPPs and not for other antimicrobial peptides which promote the immune response[5, 60]. It is clear, however, that the

data in this investigation indicate that SNAPPs have an immunomodulatory role and enhance the bactericidal activity of neutrophils.

Discussion

Though SNAPPs have exhibited a remarkable efficiency to combat Gram-negative pathogens [19, 32], our designed mixed culture studies of *E. coli* and *S. aureus* or MRSA showed the preferential targeting of Gram-positive bacteria by SNAPPs and in particular $S8_M$ over $S16_M$ which has been shown to favour Gram-negative bacteria. The strain-preference and promising potency of SNAPPs through their structure design offers guidance for the future development of clinical therapeutics in combating antimicrobial resistance. We have developed a series of star-shaped polymers, SNAPPs, potent against virulent Gram-positive MDR bacteria, including *S. aureus* and MRSA, followed by a detailed study of their mechanism. From the assessed SNAPP panel, the $S8_M$ and $S16_M$ SNAPPs were found to possess greater antimicrobial activity with $S8_M$ being a lead candidate for clinical development against *S. aureus* and MRSA infections. Our studies showed that the initial interaction process of SNAPP killing involves binding to LTA on the cell surface of *S. aureus* and MRSA, followed by translocation and insertion into the cytoplasmic membrane, leading to membrane depolarisation, inhibition of efflux pump and ROS production within minutes of SNAPP contact. A thermodynamic interaction ITC assay with direct titration of *E. coli* LPS; *S. aureus* LTA or *S. aureus* PG against SNAPP $S8_M$ and $S16_M$ showed that the $S16_M$ had higher binding affinity for the outer layer components of *E. coli* and *S. aureus* than $S8_M$ thus causing more disruption in the cell envelope of Gram-negative bacteria but being retarded in Gram-positive bacteria outer layer. This has the consequence that $S16_M$ has a slower killing time than $S8_M$ *S. aureus* and as such $S8_M$ has high antimicrobial efficacy than $S16_M$. In addition, the more helical $S8_M$ and $S16_M$ (determined by circular dichroism in Figure S19 and Table S6) than the shorter armed SNAPPs [32] can separate their amphiphilic moieties and provide an increased concentration of positive charges

in the microenvironment of the cell wall, possibly assisting cytoplasmic membrane targeting and insertion. The higher α-helical contents of both $S8_M$ and $S16_M$ in hydrophobic environment (**Figure S19**) may expose the positive charged Lys residue which can contribute their strong binding affinity with negatively charged cell components of Gram-positive bacteria (**Figure S11**). Such interaction with cells will then lead the membrane destabilization and damage, as shown in HIM images (**Figure 7**) with a clear visualisation of their membrane interaction at sub-lethal and lethal doses. The bactericidal kinetic analysis further implied the membrane depolarisation, efflux pump inhibition and ROS occurred simultaneously, which led to the cell death of *S. aureus* and MRSA in under a minute at high concentrations of SNAPP. Importantly, both $S8_M$ and $S16_M$ can significantly reduce CFU by 98.5% (2-log reduction) in both *S. aureus* and MRSA-infected mice, which corresponded with a neutrophil increase indicating that SNAPPs may have an immunomodulatory function. Given the awareness of selective/targetable antibacterial therapy by using peptide-based polymers, polymer based delivery system or photothermal therapy-derived treatment have been applied to deliver antibiotic specifically or synergistic antimicrobials for argetable treatment to combat bacterial infections[61-62]. Our current work demonstrated the multi-modal mechanisms of action with preferentially strong binding to LTA (Gram-positive), which showed prospective potency of the SNAPP structure with less haemolytic activity provide a promising direct approach to target *S. aureus*, and especially MRSA, with less potential to induce *de novo* resistance in combating the emerging threat of antimicrobial resistance.

Conclusion

Multi-drug resistant (MDR) pathogens are a recognised threat to public health, and the development of novel antibiotic alternatives to combat the infections caused by Gram-positive MDR bacteria, such as methicillin-resistant *S. aureus* (MRSA), is urgently needed. In this work, we investigated a novel antibacterial agent, the Star-Shaped "Structurally Nanoengineered

Antimicrobial Peptide Polymers" (SNAPPs) against Gram-positive bacterial infections. In a mixed culture antimicrobial assay $S16_M$ (16 arms) and to a greater extent $S8_M$ (8 arms) preferentially killed *S. aureus* or MRSA rather than *E. coli.* A panel of SNAPPs with different number of arms (4, 8 and 16 arms) and different arm lengths were fabricated and their antibacterial activity against Gram-positive *S. aureus* and MRSA was investigated. The results showed that both arm number and length were found to be critical in the SNAPP's antimicrobial activity against *S. aureus* and MRSA, with the medium arm length for the 8-arm ($S8_M$) and 16-arm ($S16_M$) being the most active. The $S8_M$ strongly interacted and bound with *S. aureus* lipoteichoic acid and killed *S. aureus* and MRSA within 10 and 30 minutes compared to $S16_M$'s 60 and 30 minutes (respectively), suggesting specific mechanisms of attachment and killing. Both $S8_M$ and $S16_M$ can induce membrane depolarisation, reduce efflux pump activity and induce reactive oxygen species. In the mouse acute peritonitis model both $S8_M$ and $S16_M$ protected animals from *S. aureus* and MRSA infection, enabling a 2-log reduction (>99%) in infection, indicating *in vivo* bactericidal activity. These data indicate that by tuning SNAPP architecture it is possible to target specific bacteria, which would significantly aid in the development of polypeptide-based antibacterial agents as well as peptide mimetic polymers against Gram-positive bacterial pathogens in polymicrobial environment.

Author contributions

W.L., G.G.Q. and N.M.O. designed research; W.L., A.R.M., S.H., J.H., J.L., S.J.S., A.B. and T.H. performed research; W.L., A.R.M., S.H., J.H. and J.L. analyzed data; and W.L., A.R.M., J.H., J.L., E.C.R., G.G.Q. and N.M.O. wrote the paper.

Supplemental information

Supplemental Information, including materials, therapeutic index, Atto 488-labelled SNAPPs, Characterisation of synthetic $S16_M$, Membrane potential flow cytometric graphs,

Representative graph of the flow cytometry of ROS, the inhibition concentration of LTA or PG, The flow cytometric graphs of neutrophils, Antibacterial activity of SNAPPs in μg/mL, MDC of mixed cultures, ITC analysis, CD structure and haemolysis activity can be found with this article.

Acknowledgments

The National Health and Medical Research Council (NHMRC) of Australia and Australian Research Council (ARC) are thanked for financial support over many years for the peptide chemistry and chemical biology studies reported in the authors' laboratories. NMOS is the recipient of NHMRC funding (APP1142472, APP1158841, APP1185426), ARC funding (DP210102781, DP160101312, LE200100163), Cancer Council Victoria funding (APP1163284) and Australian Dental Research Funding in antimicrobial materials and research is supported by the Centre for Oral Health Research at The Melbourne Dental School. We acknowledge the Melbourne Cytometry Platform (Melbourne Dental School, The University of Melbourne) for provision of flow cytometry services. The HIM work and fluorescent imaging was performed in part at the Materials Characterisation and Fabrication Platform (MCFP) at the University of Melbourne and the Victorian Node of the Australian National Fabrication Facility (ANFF).

Declaration of interests

The authors declare no conflict of interest.

References

(1) Shore, C. K.; Coukell, A. Roadmap for Antibiotic Discovery. *Nat. Microbiol.* **2016,** *1* (6), 16083.

(2) Organization, W. H. Antimicrobial Resistance: Global Report on Surveillance. *World Health Organization, Geneva, Switzerland* **2014**.

(3) Lepore, C.; Silver, L.; Theuretzbacher, U.; Thomas, J.; Visi, D. The Small-Molecule Antibiotics Pipeline: 2014-2018. *Nat. Rev. Drug Discov.* **2019,** *18* (10), 739.

(4) Hede, K. Antibiotic Resistance: An Infectious Arms Race. *Nature* **2014,** *509* (7498), S2-S3.

(5) Li, W.; Tailhades, J.; O'Brien-Simpson, N.; Separovic, F.; Otvos, L., Jr.; Hossain, M. A.; Wade, J. Proline-Rich Antimicrobial Peptides: Potential Therapeutics against Antibiotic-Resistant Bacteria. *Amino Acids* **2014,** *46* (10), 2287-2294.

(6) Fernandes, P.; Martens, E. Antibiotics in Late Clinical Development. *Biochem. Pharmacol.* **2017,** *133*, 152-163.

(7) O'Neill, J. Antimicrobial Resistance https://amr-review.org/ (accessed 5 Jan).

(8) Tacconelli, E.; Carrara, E.; Savoldi, A.; Harbarth, S.; Mendelson, M.; Monnet, D. L.; Pulcini, C.; Kahlmeter, G.; Kluytmans, J.; Carmeli, Y.; Ouellette, M.; Outterson, K.; Patel, J.; Cavaleri, M.; Cox, E. M.; Houchens, C. R.; Grayson, M. L.; Hansen, P.; Singh, N.; Theuretzbacher, U.; Magrini, N.; Aboderin, A. O.; Al-Abri, S. S.; Awang Jalil, N.; Benzonana, N.; Bhattacharya, S.; Brink, A. J.; Burkert, F. R.; Cars, O.; Cornaglia, G.; Dyar, O. J.; Friedrich, A. W.; Gales, A. C.; Gandra, S.; Giske, C. G.; Goff, D. A.; Goossens, H.; Gottlieb, T.; Guzman Blanco, M.; Hryniewicz, W.; Kattula, D.; Jinks, T.; Kanj, S. S.; Kerr, L.; Kieny, M.-P.; Kim, Y. S.; Kozlov, R. S.; Labarca, J.; Laxminarayan, R.; Leder, K.; Leibovici, L.; Levy-Hara, G.; Littman, J.; Malhotra-Kumar, S.; Manchanda, V.; Moja, L.; Ndoye, B.; Pan, A.; Paterson, D. L.; Paul, M.; Qiu, H.; Ramon-Pardo, P.; Rodríguez-Baño, J.; Sanguinetti, M.; Sengupta, S.; Sharland, M.; Si-Mehand, M.; Silver, L. L.; Song, W.; Steinbakk, M.; Thomsen, J.; Thwaites, G. E.; van der Meer, J. W. M.; Van Kinh, N.; Vega, S.; Villegas, M. V.; Wechsler-Fördös, A.; Wertheim, H. F. L.; Wesangula, E.; Woodford, N.; Yilmaz, F. O.; Zorzet, A. Discovery, Research, and Development of New Antibiotics: The Who Priority List of Antibiotic-Resistant Bacteria and Tuberculosis. *Lancet Infect Dis* **2018,** *18* (3), 318-327.

(9) Lakhundi, S.; Zhang, K. Methicillin-Resistant Staphylococcus Aureus: Molecular Characterization, Evolution, and Epidemiology. *Clin. Microbiol. Rev.* **2018,** *31* (4), e00020-18.

(10) Lowy, F. D. Staphylococcus Aureus Infections. *N. Engl. J. Med.* **1998,** *339* (8), 520-532.

(11) Appelbaum, P. C. Microbiology of Antibiotic Resistance in Staphylococcus Aureus. *Clin. Infect. Dis.* **2007,** *45* (Supplement_3), S165-S170.
(12) Holland, T. L.; Arnold, C.; Fowler, V. G., Jr. Clinical Management of Staphylococcus Aureus Bacteremia: A Review. *JAMA* **2014,** *312* (13), 1330-1341.
(13) Liu, W.-T.; Chen, E.-Z.; Yang, L.; Peng, C.; Wang, Q.; Xu, Z.; Chen, D.-Q. Emerging Resistance Mechanisms for 4 Types of Common Anti-Mrsa Antibiotics in Staphylococcus Aureus: A Comprehensive Review. *Microb. Pathog.* **2021,** *156*, 104915.
(14) Kumar, K.; Chopra, S. New Drugs for Methicillin-Resistant Staphylococcus Aureus: An Update. *J. Antimicrob. Chemother.* **2013,** *68* (7), 1465-1470.
(15) Rasines Mazo, A.; Allison-Logan, S.; Karimi, F.; Chan, N. J.-A.; Qiu, W.; Duan, W.; O'Brien-Simpson, N. M.; Qiao, G. G. Ring Opening Polymerization of A-Amino Acids: Advances in Synthesis, Architecture and Applications of Polypeptides and Their Hybrids. *Chem. Soc. Rev.* **2020,** *49*, 4737-4834
(16) Li, W.; Separovic, F.; O'Brien-Simpson, N. M.; Wade, J. D. Chemically Modified and Conjugated Antimicrobial Peptides against Superbugs. *Chem. Soc. Rev.* **2021,** *50* (8), 4932-4973.
(17) Czaplewski, L.; Bax, R.; Clokie, M.; Dawson, M.; Fairhead, H.; Fischetti, V. A.; Foster, S.; Gilmore, B. F.; Hancock, R. E. W.; Harper, D.; Henderson, I. R.; Hilpert, K.; Jones, B. V.; Kadioglu, A.; Knowles, D.; Ólafsdóttir, S.; Payne, D.; Projan, S.; Shaunak, S.; Silverman, J.; Thomas, C. M.; Trust, T. J.; Warn, P.; Rex, J. H. Alternatives to Antibiotics - a Pipeline Portfolio Review. *Lancet Infect Dis* **2016,** *16* (2), 239-251.
(18) Fjell, C. D.; Hiss, J. A.; Hancock, R. E. W.; Schneider, G. Designing Antimicrobial Peptides: Form Follows Function. *Nat. Rev. Drug Discov.* **2011,** *11*, 37.
(19) Lam, S. J.; O'Brien-Simpson, N. M.; Pantarat, N.; Sulistio, A.; Wong, E. H. H.; Chen, Y.-Y.; Lenzo, J. C.; Holden, J. A.; Blencowe, A.; Reynolds, E. C.; Qiao, G. G. Combating Multidrug-Resistant Gram-Negative Bacteria with Structurally Nanoengineered Antimicrobial Peptide Polymers. *Nat. Microbiol.* **2016,** *1*, 16162.
(20) Lam, S. J.; Wong, E. H. H.; O'Brien-Simpson, N. M.; Pantarat, N.; Blencowe, A.; Reynolds, E. C.; Qiao, G. G. Bionano Interaction Study on Antimicrobial Star-Shaped Peptide Polymer Nanoparticles. *ACS Appl. Mater. Interfaces* **2016,** *8* (49), 33446-33456.
(21) Pranantyo, D.; Xu, L. Q.; Hou, Z.; Kang, E.-T.; Chan-Park, M. B. Increasing Bacterial Affinity and Cytocompatibility with Four-Arm Star Glycopolymers and Antimicrobial A-Polylysine. *Polym. Chem.* **2017,** *8* (21), 3364-3373.

(22) Chen, Y.-F.; Lai, Y.-D.; Chang, C.-H.; Tsai, Y.-C.; Tang, C.-C.; Jan, J.-S. Star-Shaped Polypeptides Exhibit Potent Antibacterial Activities. *Nanoscale* **2019,** *11* (24), 11696-11708.
(23) Wong, E. H. H.; Khin, M. M.; Ravikumar, V.; Si, Z.; Rice, S. A.; Chan-Park, M. B. Modulating Antimicrobial Activity and Mammalian Cell Biocompatibility with Glucosamine-Functionalized Star Polymers. *Biomacromolecules* **2016,** *17* (3), 1170-1178.
(24) Liu, H.; Zhang, X.; Zhao, Z.; Yang, F.; Xue, R.; Yin, L.; Song, Z.; Cheng, J.; Luan, S.; Tang, H. Efficient Synthesis and Excellent Antimicrobial Activity of Star-Shaped Cationic Polypeptides with Improved Biocompatibility. *Biomater. Sci.* **2021,** *9* (7), 2721-2731.
(25) Chen, Y.; Yu, L.; Zhang, B.; Feng, W.; Xu, M.; Gao, L.; Liu, N.; Wang, Q.; Huang, X.; Li, P.; Huang, W. Design and Synthesis of Biocompatible, Hemocompatible, and Highly Selective Antimicrobial Cationic Peptidopolysaccharides Via Click Chemistry. *Biomacromolecules* **2019,** *20* (6), 2230-2240.
(26) Li, P.; Zhou, C.; Rayatpisheh, S.; Ye, K.; Poon, Y. F.; Hammond, P. T.; Duan, H.; Chan-Park, M. B. Cationic Peptidopolysaccharides Show Excellent Broad-Spectrum Antimicrobial Activities and High Selectivity. *Adv. Mater. (Weinheim, Ger.)* **2012,** *24* (30), 4130-4137.
(27) Zhou, C.; Qi, X.; Li, P.; Chen, W. N.; Mouad, L.; Chang, M. W.; Leong, S. S. J.; Chan-Park, M. B. High Potency and Broad-Spectrum Antimicrobial Peptides Synthesized Via Ring-Opening Polymerization of A-Aminoacid-N-Carboxyanhydrides. *Biomacromolecules* **2010,** *11* (1), 60-67.
(28) Ding, X.; Yang, C.; Moreira, W.; Yuan, P.; Periaswamy, B.; de Sessions, P. F.; Zhao, H.; Tan, J.; Lee, A.; Ong, K. X.; Park, N.; Liang, Z. C.; Hedrick, J. L.; Yang, Y. Y. A Macromolecule Reversing Antibiotic Resistance Phenotype and Repurposing Drugs as Potent Antibiotics. *Advanced Science* **2020,** *7* (17), 2001374.
(29) Bai, S.; Wang, J.; Yang, K.; Zhou, C.; Xu, Y.; Song, J.; Gu, Y.; Chen, Z.; Wang, M.; Shoen, C.; Andrade, B.; Cynamon, M.; Zhou, K.; Wang, H.; Cai, Q.; Oldfield, E.; Zimmerman, S. C.; Bai, Y.; Feng, X. A Polymeric Approach toward Resistance-Resistant Antimicrobial Agent with Dual-Selective Mechanisms of Action. *Adv. Healthc. Mater.* **2021,** *7* (5), eabc9917.
(30) Tan, J.; Zhao, Y.; Hedrick, J. L.; Yang, Y. Y. Effects of Hydrophobicity on Antimicrobial Activity, Selectivity, and Functional Mechanism of Guanidinium-Functionalized Polymers. *Science Advances* **2021,** *7* (5), 2100482.
(31) Zhang, Y.; Song, W.; Li, S.; Kim, D.-K.; Kim, J. H.; Kim, J. R.; Kim, I. Facile and Scalable Synthesis of Topologically Nanoengineered Polypeptides with Excellent Antimicrobial Activities. *Chem. Commun.* **2020,** *56* (3), 356-359.

(32) Shirbin, S. J.; Insua, I.; Holden, J. A.; Lenzo, J. C.; Reynolds, E. C.; O'Brien-Simpson, N. M.; Qiao, G. G. Architectural Effects of Star-Shaped "Structurally Nanoengineered Antimicrobial Peptide Polymers" (Snapps) on Their Biological Activity. *Adv. Healthc. Mater.* **2018,** *7*, 1800627.

(33) Li, W.; Lin, F.; Hung, A.; Barlow, A.; Sani, M.-A.; Paolini, R.; Singleton, W.; Holden, J.; Hossain, M. A.; Separovic, F.; O'Brien-Simpson, N. M.; Wade, J. D. Enhancing Proline-Rich Antimicrobial Peptide Action by Homodimerization: Influence of Bifunctional Linker. *Chem. Sci.* **2022,** *13* (8), 2226-2237.

(34) Koehbach, J.; Craik, D. J. The Vast Structural Diversity of Antimicrobial Peptides. *Trends Pharmacol. Sci.* **2019,** *40* (7), 517-528.

(35) Li, W.; O'Brien-Simpson, N. M.; Tailhades, J.; Pantarat, N.; Dawson, R. M.; Otvos, L., Jr.; Reynolds, E. C.; Separovic, F.; Hossain, M. A.; Wade, J. D. Multimerization of a Proline-Rich Antimicrobial Peptide, Chex-Arg20, Alters Its Mechanism of Interaction with the Escherichia Coli Membrane. *Chem. Biol.* **2015,** *22* (9), 1250-1258.

(36) O'Brien-Simpson, N. M.; Pantarat, N.; Attard, T. J.; Walsh, K. A.; Reynolds, E. C. A Rapid and Quantitative Flow Cytometry Method for the Analysis of Membrane Disruptive Antimicrobial Activity. *PLoS One* **2016,** *11* (3), e0151694.

(37) Li, W.; O'Brien‐Simpson, N. M.; Holden, J. A.; Otvos, L.; Reynolds, E. C.; Separovic, F.; Hossain, M. A.; Wade, J. D. Covalent Conjugation of Cationic Antimicrobial Peptides with a β‐Lactam Antibiotic Core. *Pep. Sci.* **2018,** *110* (3), e24059.

(38) Li, W.; O'Brien-Simpson, N. M.; Yao, S.; Tailhades, J.; Reynolds, E. C.; Dawson, R. M.; Otvos, L.; Hossain, M. A.; Separovic, F.; Wade, J. D. C-Terminal Modification and Multimerization Increase the Efficacy of a Proline-Rich Antimicrobial Peptide. *Chem. Eur. J.* **2017,** *23*, 390-396.

(39) ASTM. *Astm E2315-16, Standard Guide for Assessment of Antimicrobial Activity Using a Time-Kill Procedure,*, ASTM International ed.; West Conshohocken: 2016.

(40) Dejager, L.; Pinheiro, I.; Dejonckheere, E.; Libert, C. Cecal Ligation and Puncture: The Gold Standard Model for Polymicrobial Sepsis? *Trends Microbiol.* **2011,** *19* (4), 198-208.

(41) Oh, J. K.; Yegin, Y.; Yang, F.; Zhang, M.; Li, J.; Huang, S.; Verkhoturov, S. V.; Schweikert, E. A.; Perez-Lewis, K.; Scholar, E. A.; Taylor, T. M.; Castillo, A.; Cisneros-Zevallos, L.; Min, Y.; Akbulut, M. The Influence of Surface Chemistry on the Kinetics and Thermodynamics of Bacterial Adhesion. *Sci. Rep.* **2018,** *8* (1), 17247.

(42) Benarroch, J. M.; Asally, M. The Microbiologist's Guide to Membrane Potential Dynamics. *Trends Microbiol.* **2020,** *28* (4), 304-314.
(43) Hobbs, J. K.; Miller, K.; O'Neill, A. J.; Chopra, I. Consequences of Daptomycin-Mediated Membrane Damage in Staphylococcus Aureus. *J. Antimicrob. Chemother.* **2008,** *62* (5), 1003-1008.
(44) Zhao, X.; Drlica, K. Reactive Oxygen Species and the Bacterial Response to Lethal Stress. *Curr. Opin. Microbiol.* **2014,** *21*, 1-6.
(45) Brynildsen, M. P.; Winkler, J. A.; Spina, C. S.; MacDonald, I. C.; Collins, J. J. Potentiating Antibacterial Activity by Predictably Enhancing Endogenous Microbial Ros Production. *Nat. Biotechnol.* **2013,** *31* (2), 160-165.
(46) Lam, P. L.; Wong, R. S. M.; Lam, K. H.; Hung, L. K.; Wong, M. M.; Yung, L. H.; Ho, Y. W.; Wong, W. Y.; Hau, D. K. P.; Gambari, R.; Chui, C. H. The Role of Reactive Oxygen Species in the Biological Activity of Antimicrobial Agents: An Updated Mini Review. *Chem. Biol. Interact.* **2020,** *320*, 109023.
(47) Hong, Y.; Zeng, J.; Wang, X.; Drlica, K.; Zhao, X. Post-Stress Bacterial Cell Death Mediated by Reactive Oxygen Species. *Proc. Natl. Acad. Sci. U. S. A.* **2019,** *116* (20), 10064-10071.
(48) Fischer, W.; Mannsfeld, T.; Hagen, G. On the Basic Structure of Poly (Glycerophosphate) Lipoteichoic Acids. *Biochem. Cell Biol.* **1990,** *68* (1), 33-43.
(49) Joens, M. S.; Huynh, C.; Kasuboski, J. M.; Ferranti, D.; Sigal, Y. J.; Zeitvogel, F.; Obst, M.; Burkhardt, C. J.; Curran, K. P.; Chalasani, S. H.; Stern, L. A.; Goetze, B.; Fitzpatrick, J. A. J. Helium Ion Microscopy (Him) for the Imaging of Biological Samples at Sub-Nanometer Resolution. *Sci. Rep.* **2013,** *3* (1), 3514.
(50) Lin, B.; Hung, A.; Li, R.; Barlow, A.; Singleton, W.; Matthyssen, T.; Sani, M.-A.; Hossain, M. A.; Wade, J. D.; O'Brien-Simpson, N. M.; Li, W. Systematic Comparison of Activity and Mechanism of Antimicrobial Peptides against Nosocomial Pathogens. *Eur. J. Med. Chem.* **2022,** *231* (114135), 114135.
(51) Bitto, N. J.; Cheng, L.; Johnston, E. L.; Pathirana, R.; Phan, T. K.; Poon, I. K. H.; O'Brien-Simpson, N. M.; Hill, A. F.; Stinear, T. P.; Kaparakis-Liaskos, M. Staphylococcus Aureus Membrane Vesicles Contain Immunostimulatory DNA, Rna and Peptidoglycan That Activate Innate Immune Receptors and Induce Autophagy. *J. Extracell. Vesicles* **2021,** *10* (6), e12080.
(52) Du, D.; Wang-Kan, X.; Neuberger, A.; van Veen, H. W.; Pos, K. M.; Piddock, L. J. V.; Luisi, B. F. Multidrug Efflux Pumps: Structure, Function and Regulation. *Nat. Rev. Microbiol.* **2018,** *16* (9), 523-539.

(53) Fernández, L.; Hancock, R. E. W. Adaptive and Mutational Resistance: Role of Porins and Efflux Pumps in Drug Resistance. *Clin. Microbiol. Rev.* **2012,** *25* (4), 661-681.
(54) Jaradat, D. s. M. M.; Al-Karablieh, N.; Zaarer, B. H. M.; Li, W.; Saleh, K. K. Y.; Rasras, A. J.; Abu-Romman, S.; O'Brien-Simpson, N. M.; Wade, J. D. Human Glucose-Dependent Insulinotropic Polypeptide (Gip) Is an Antimicrobial Adjuvant Re-Sensitising Multidrug-Resistant Gram-Negative Bacteria. *Biol. Chem.* **2021,** *402* (4), 513-524.
(55) Paixão, L.; Rodrigues, L.; Couto, I.; Martins, M.; Fernandes, P.; de Carvalho, C. C. C. R.; Monteiro, G. A.; Sansonetty, F.; Amaral, L.; Viveiros, M. Fluorometric Determination of Ethidium Bromide Efflux Kinetics in Escherichia Coli. *J. Biol. Eng.* **2009,** *3* (1), 18.
(56) Sánchez-Romero, M. A.; Casadesús, J. Contribution of Phenotypic Heterogeneity to Adaptive Antibiotic Resistance. *Proc. Natl. Acad. Sci. U. S. A.* **2014,** *111* (1), 355-360.
(57) Blair, J. M. A.; Piddock, L. J. V. How to Measure Export Via Bacterial Multidrug Resistance Efflux Pumps. *mBio* **2016,** *7* (4), e00840-16.
(58) Neelay, O. P.; Peterson, C. A.; Snavely, M. E.; Brown, T. C.; TecleMariam, A. F.; Campbell, J. A.; Blake, A. M.; Schneider, S. C.; Cremeens, M. E. Antimicrobial Peptides Interact with Peptidoglycan. *J. Mol. Struct.* **2017,** *1146*, 329-336.
(59) Scott, M. G.; Gold, M. R.; Hancock, R. E. W. Interaction of Cationic Peptides with Lipoteichoic Acid and Gram-Positive Bacteria. *Infect. Immun.* **1999,** *67* (12), 6445-6453.
(60) Hancock, R. E. W.; Haney, E. F.; Gill, E. E. The Immunology of Host Defence Peptides: Beyond Antimicrobial Activity. *Nat. Rev. Immunol.* **2016,** *16* (5), 321-334.
(61) Huo, J.; Jia, Q.; Huang, H.; Zhang, J.; Li, P.; Dong, X.; Huang, W. Emerging Photothermal-Derived Multimodal Synergistic Therapy in Combating Bacterial Infections. *Chem. Soc. Rev.* **2021,** *50* (15), 8762-8789.
(62) Wang, T.; Rong, F.; Tang, Y.; Li, M.; Feng, T.; Zhou, Q.; Li, P.; Huang, W. Targeted Polymer-Based Antibiotic Delivery System: A Promising Option for Treating Bacterial Infections Via Macromolecular Approaches. *Prog. Polym. Sci.* **2021,** *116*, 101389.

Graphic Abstract